#### **Review Article**

Sheikha A. Alkhursani, Nadiah Yousef Aldaleeli, Samera Ali Al-Gahtany, Mohamed Mohamady Ghobashy\*, Sarah Alharthi, Lamiaa Galal Amin, Safwat A. Mahmoud, Waleed E. Boraie, Mohamed S. Attia, and Mohamed Madani\*

# Future prospects of gold nanoclusters in hydrogen storage systems and sustainable environmental treatment applications

https://doi.org/10.1515/ntrev-2024-0087 received September 15, 2023; accepted July 26, 2024

Abstract: Gold nanoclusters (AuNCs), with sizes below 2 nm, have emerged as remarkable nanomaterials exhibiting unique optical, electronic, and chemical properties. Their ultra-small size imparts advantageous characteristics, including high surface area, tunable fluorescence, and excellent biocompatibility, making AuNCs highly promising for diverse applications. This article explores recent advancements in leveraging AuNCs to address critical challenges in clean energy storage and environmental remediation. For energy storage, AuNCs boost the performance of Li-based batteries by facilitating rapid electron transfer kinetics and limiting polysulfide shuttling. The review delves into mechanistic insights governing AuNC-hydrogen interactions, various synthetic approaches for tailoring AuNCs, and

their emerging applications as advanced electrodes, efficient catalysts, and conductive additives enabling improved charge storage capabilities. Additionally, using plasmonic effects and hot carrier generation induced by AuNCs shows tremendous potential in photocatalytic water splitting for clean hydrogen fuel production. For environmental applications, AuNCs enable the degradation of persistent organic pollutants, heavy metal ion detection at part-per-trillion levels, and solar-driven water purification, relying on plasmonenhanced hot carrier processes. However, the long-term ecological impacts of AuNCs remain unclear. This study thus underscores the need for further toxicological assessments and life cycle analyses to promote sustainable AuNC-based technologies through responsible research and innovation. Overall, it highlights the versatile applicability of AuNCs in addressing critical energy and environmental challenges.

**Keywords:** gold nanoclusters, clean energy storage, environmental remediation, plasmonic effects

Sheikha A. Alkhursani, Nadiah Yousef Aldaleeli: College of Science and Humanities - Jubail, Imam Abdulrahman Bin Faisal University, Jubail, Saudi Arabia

Samera Ali Al-Gahtany: Faculty of Science, University of Jeddah, Jeddah, 21959, Saudi Arabia

Sarah Alharthi: Department of Chemistry, College of Science, Taif University, P.O. Box 11099, Taif, 21944, Saudi Arabia

Lamiaa Galal Amin, Safwat A. Mahmoud: Physics Department, Faculty of Science, Northern Border University, Arar, Saudi Arabia

Waleed E. Boraie: Department of Chemistry, College of Science, King Faisal University, P.O. Box 400, Al-Ahsa, 31982, Saudi Arabia Mohamed S. Attia: Chemistry Department, Faculty of Science, Ain

Shams University, Abbassia, Cairo, 11566, Egypt

ORCID: Mohamed Mohamady Ghobashy 0000-0003-0968-1423;

Mohamed Madani 0000-0003-3434-6301

### 1 Introduction

Gold nanoclusters (AuNCs) possess several vital properties that contribute to their versatility. Their ultra-small size imparts a high surface area, allowing for increased reactivity and interactions with surrounding environments [1]. Applying gold nanoparticles (GNPs) in hydrogen storage represents a promising and innovative avenue for efficient and sustainable energy solutions [2]. Hydrogen has emerged as a critical contender in the pursuit of clean energy, owing to its abundance and potential as a highenergy-density fuel [3]. However, the practical hydrogen storage remains a significant challenge, requiring advanced materials and technologies. In this context, GNPs showcase unique properties that position them as compelling candidates for enhancing hydrogen storage systems [4].

<sup>\*</sup> Corresponding author: Mohamed Mohamady Ghobashy, Radiation Research of Polymer Chemistry Department, National Center for Radiation Research and Technology (NCRRT), Atomic Energy Authority, P.O. Box 8029, Nasr City, Cairo, Egypt, e-mail: Mohamed\_Ghobashy@yahoo.com

<sup>\*</sup> Corresponding author: Mohamed Madani, College of Science and Humanities - Jubail, Imam Abdulrahman Bin Faisal University, Jubail, Saudi Arabia, e-mail: mmadani@iau.edu.sa

GNPs exhibit extraordinary catalytic activity, and their surface properties can be finely tuned for optimal hydrogen adsorption and desorption kinetics [5]. The large surface area of GNPs provides ample sites for hydrogen molecules to interact, facilitating improved storage capacity [6]. Moreover, the tunable size and shape of GNPs enable the customization of their electronic and geometric characteristics, further influencing their interaction with hydrogen [7]. GNP-assisted hydrogen storage explores the quantum size effects and surface phenomena that govern their behavior [8]. Additionally, it outlines various synthesis methods employed to fabricate GNPs with tailored properties conducive to efficient hydrogen storage. The subsequent sections will navigate the current and emerging applications of GNPs in hydrogen storage, encompassing advancements in materials science and catalysis [9]. As researchers bridge the gap between theory and applications in the realm of plasmonic nanoparticles (NPs), utilizing GNPs in hydrogen storage stands out as a testament to interdisciplinary efforts to address critical energy challenges [10]. This study not only sheds light on the theoretical and practical aspects of GNP-assisted hydrogen storage but also underscores the transformative potential of this technology in shaping the future of clean and sustainable energy systems [7]. The tunable fluorescence of AuNCs, stemming from quantum size effects, provides a unique optical signature, enabling applications in sensing and imaging [11]. Additionally, their excellent biocompatibility, ease of functionalization, and environmental stability further enhance their appeal for various applications [12]. Recent research has highlighted significant findings in environmental pollution and advanced material applications [13-15]. This is complemented by exploring innovative eco-friendly materials for environmental application, demonstrating high efficacy [16–19]. The synthesis of AuNCs has witnessed significant progress, with diverse methods developed to tailor their size, shape, and surface properties [20]. Typical approaches involve chemical reduction, electrochemical processes, and stabilizing ligands, allowing precise control over the nanocluster's characteristics [21]. AuNCs have shown promise as catalysts for various chemical reactions, including fuel cells' oxygen reduction reaction (ORR) [22]. Their high catalytic activity, stability, and low cost make them attractive alternatives to traditional catalysts [23]. The unique electronic properties of AuNCs contribute to their application in supercapacitors [24]. Their high conductivity and electrochemical stability enhance the performance of supercapacitor devices, offering efficient energy storage solutions [25]. Their use as electrode materials or as components in battery electrolytes has demonstrated improved energy storage capabilities. AuNCs exhibit catalytic activity in the degradation of environmental pollutants [26]. Their ability

to activate specific reactions can be harnessed to remove organic contaminants from water and air [27]. The tunable fluorescence of AuNCs makes them ideal candidates for sensors in environmental monitoring [28]. They can be engineered to detect specific pollutants, providing a rapid and sensitive analytical tool [29]. AuNCs have demonstrated photocatalytic properties, enabling the degradation of contaminants under light irradiation [30]. This approach holds promise for the development of sustainable and energy-efficient remediation technologies. Understanding the underlying mechanisms governing the applications of AuNCs is crucial for optimizing their performance. The quantum size effects, surface chemistry, and electronic structure of AuNCs are pivotal in dictating their behavior in energy storage and environmental remediation processes. Tailoring these properties through precise synthesis methods is critical to harnessing the full potential of AuNCs in diverse applications. While the potential applications of AuNCs in energy storage and environmental remediation are promising, addressing safety and ethical concerns is essential. The impact of AuNCs on human health and the environment [13], along with their life cycle analysis, must be thoroughly evaluated. Responsible research practices, transparent reporting of findings, and adherence to ethical standards are imperative for the sustainable development of AuNC-based technologies. AuNCs have emerged as versatile nanomaterials with unique properties that make them well-suited for energy storage and environmental remediation applications [31]. The recent advances in AuNC research highlight their potential in catalysis, supercapacitors, pollutant degradation, and environmental sensing. Understanding the underlying mechanisms governing their behavior is essential for optimizing their performance. Moreover, addressing safety and ethical considerations is crucial to ensuring the responsible development and deployment of AuNC-based technologies. As research in this field progresses, AuNCs are poised to contribute significantly to advancing sustainable energy and environmental solutions.

**DE GRUYTER** 

# 2 Featured singular properties of AuNCs with sizes below 2 nm

AuNCs with sizes below 2 nm exhibit unique and singular properties that distinguish them from larger GNPs. One striking feature is their size-dependent electronic and optical properties, often displaying discrete electronic energy levels due to quantum confinement effects [32]. This results in a distinct electronic structure, leading to size-tunable photoluminescence, making AuNCs promising for applications in sensors and imaging [33]. The small size also contributes to a

large surface-to-volume ratio, enhancing their reactivity and making them efficient catalysts for various reactions [34]. Moreover, the stability and robustness of AuNCs are remarkable, showcasing resistance to aggregation and demonstrating excellent catalytic performance even in harsh environments [35]. The precise control over their size and composition also allows for fine-tuning their properties, offering opportunities for tailoring AuNCs for specific applications in nanomedicine, catalysis, and optoelectronics. These singular features make sub-2 nm AuNCs a fascinating and versatile class of nanomaterials with tremendous potential across diverse fields [36]. AuNCs with sizes below 2 nm exhibit unique and fascinating properties that distinguish them from larger GNPs [37]. Here, we delve into the singular features of these small-sized AuNCs:

#### 2.1 Quantum size effects

The electronic structure of AuNCs is highly dependent on their size. As the size of the AuNCs approaches the nanometer scale, quantum size effects become prominent. These effects arise from quantum confinement, where the confinement of electrons and holes within the small dimensions of the AuNCs leads to discrete energy levels. Consequently, the optical and electronic properties of AuNCs can be finely tuned by controlling their size [38].

#### 2.2 Size-dependent optical properties

AuNCs exhibit size-dependent absorption and emission spectra due to quantum confinement effects. As the size decreases, the energy bandgap increases, leading to a blue shift in the absorption and emission wavelengths. This size-dependent optical behavior enables precise tuning of the plasmonic and photoluminescence properties of AuNCs, making them attractive candidates for various applications, including sensing, imaging, and optoelectronics [39].

# 2.3 High photoluminescence quantum yield

AuNCs, unlike larger GNPs, display strong and size-tunable photoluminescence. The small size and unique electronic structure of AuNCs promote the radiative recombination of excitons, resulting in efficient light emission. AuNCs can exhibit high photoluminescence quantum yields, making them

promising candidates for fluorescence-based applications, such as bioimaging and single-molecule detection [40].

#### 2.4 Atomically precise structure

AuNCs with sizes below 2 nm can be synthesized with atomic precision, enabling the synthesis of monodisperse clusters with a well-defined number of gold atoms. The precise control over the cluster size and composition allows for investigating structure-property relationships at the atomic scale. Additionally, the accurate structure of AuNCs facilitates their use as model systems for studying fundamental properties of nanomaterials [41,42].

#### 2.5 Enhanced catalytic activity

Small-sized AuNCs possess high surface-to-volume ratios, producing many exposed atoms. This property, combined with their unique electronic structure, endows AuNCs with exceptional catalytic activity. They have been demonstrated to be efficient catalysts for various reactions, including oxidation, hydrogenation, and CO oxidation. The high catalytic activity of AuNCs opens up possibilities for their utilization in energy conversion, environmental remediation, and chemical synthesis [43].

Figure 1 shows that AuNCs with sizes below 2 nm exhibit singular properties arising from quantum size effects, size-dependent optical behavior, high photoluminescence quantum yield, atomically precise structure, and enhanced catalytic activity. It emphasizes the distinct electronic properties observed at different size regimes and the emergence of quantum effects in the nanoscale range. These distinctive characteristics make AuNCs attractive for various applications, including optoelectronics, sensing, catalysis, and fundamental nanoscience research. Atomic scale (~Angstroms): atoms and diatomic molecules exhibit discrete electronic energy levels and transitions between levels.

- (1) Quantum-sized nanoclusters (1-3 nm): Contain tens to hundreds of atoms and display molecule-like properties, including the highest occupied and lowest unoccupied molecular orbitals (HOMO/LUMO), energy bandgaps  $(E_g)$ , and discrete electronic excitations.
- (2) Metallic-state NPs (3–100 nm): Properties transition toward metallic behavior with smaller bandgaps, the emergence of plasmons, continuous bands of electronic states, and collective electron excitations.

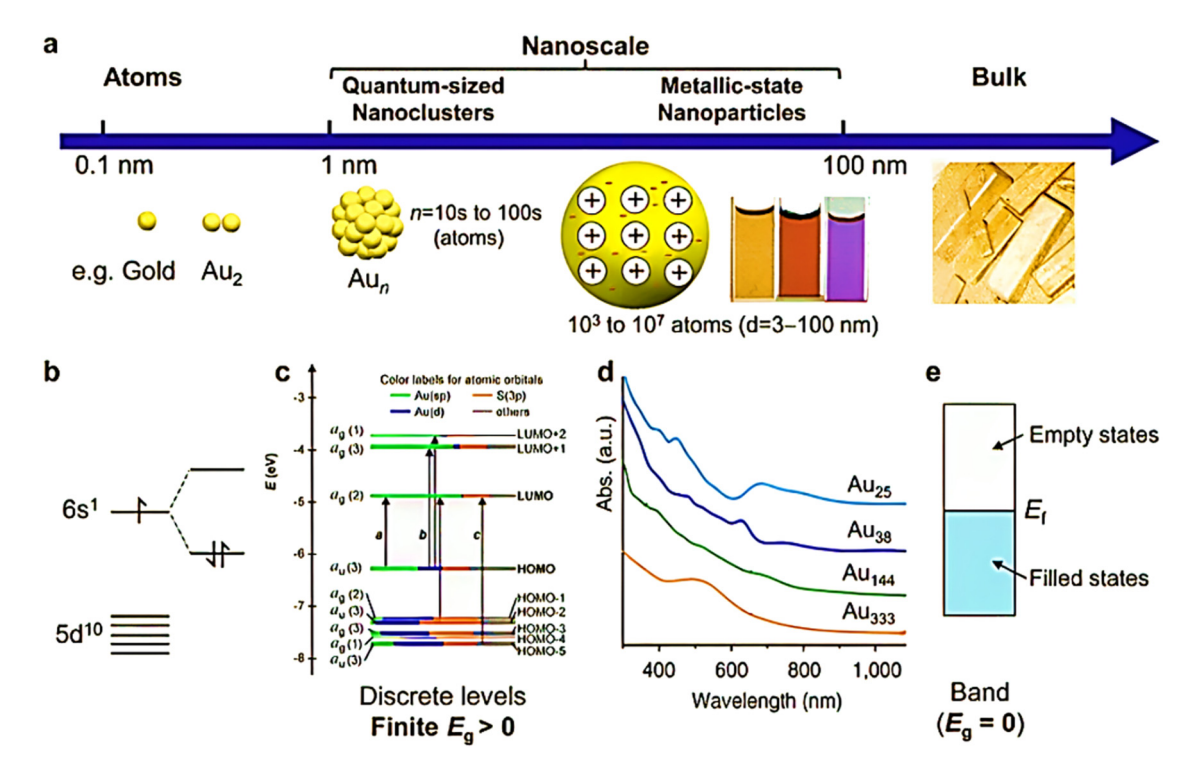
(3) Bulk metals: Possess metallic properties with continuous band structure where valence and conduction bands overlap, no bandgap, and a Fermi level.

In Figure 1a, nanoscale, ranging from 1 to 100 nm, can be divided into two distinct size regimes: quantum-sized nanoclusters (1-3 nm) consisting of tens to hundreds of atoms and regular metallic-state NPs (3-100 nm). Figure 1b shows the atomic and diatomic scale. The electronic states are discrete and localized. Figure 1c shows the quantumsized nanoclusters, the electronic structure taking on a molecule-like character. It exhibits distinct energy levels, including the HOMO and the LUMO. The energy gap between the HOMO and LUMO is denoted as  $E_g$ . Figure 1d shows that as the size of nanoclusters increases, there is an evolution from discrete electronic excitations to collective electron excitations known as plasmons. This transition is reflected in the optical absorption spectra, where larger nanoclusters exhibit plasmon resonances. Figure 1e shows the metallic-state NPs and bulk metals, and the electronic structure becomes continuous and forms energy bands. This

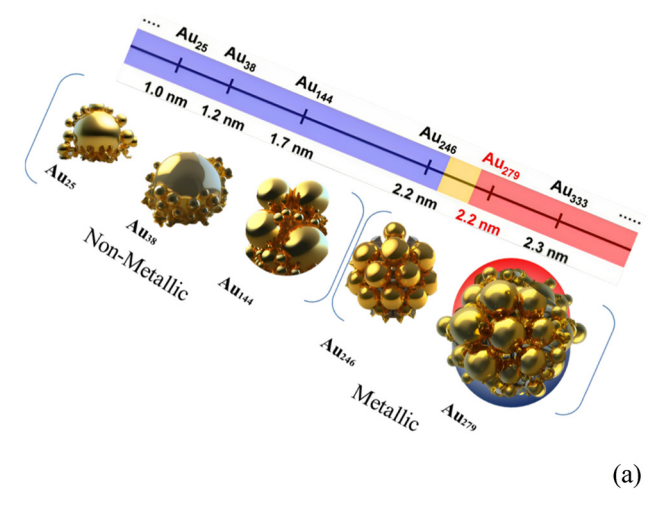
constant band electronic structure is characterized by the Fermi level/energy ( $E_{\rm f}$ ), representing the energy at which the highest occupied electronic states are found.

Exact size control allows elucidating the nonmetal-metal transition in AuNCs, resulting in emergent quantum properties in the sub-2 nm regime before classical metallic behavior takes over at slightly larger sizes. Figure 2 shows the size-dependent transition in the electronic structure and optical properties of atomically precise AuNCs ranging from Au246 to Au279. Au246 (1.4 nm size) displays a clear bandgap ( $E_{\rm g} > 0$ ), indicating non-metallic molecular behavior. Precise synthetic control elucidates the nonmetal-to-metal transition in GNPs down to the atomic level, allowing the fundamental exploration of novel size-dependent optical, electronic, and other coupled phenomena in the 1–3 nm nanocluster regime. As the size increases to Au279 (1.6 nm), the bandgap closes ( $E_{\rm g} = 0$ ), demonstrating metallicity emergence.

This sharp transition from nonmetal to metal properties occurs over an ultra-small 1.4–1.6 nm size regime in AuNCs. Optical absorption spectra similarly show the



**Figure 1:** The evolutionary journey from atomic building blocks to the nanoscale and bulk metals. (a) The nanoscale (1–100 nm) is divided into two distinct size regimes: quantum-sized nanoclusters (1–3 nm) consisting of tens to hundreds of atoms and regular metallic-state NPs (3–100 nm). (b) Atomic and diatomic electronic states serve as the foundation for understanding electronic structures. (c) Quantum-sized nanoclusters exhibit a molecule-like electronic structure characterized by the HOMO, the LUMO, and  $E_g$  (HOMO-LUMO gap). (d) The evolution from discrete electronic excitation to collective electron excitation (plasmon) is showcased in optical absorption spectra with increasing size of nanoclusters. (e) The continuous band electronic structure is illustrated for metallic-state NPs and bulk metals, featuring  $E_f$  as the Fermi level/energy. Copyright with permission from the study of Jin and Higaki [44].



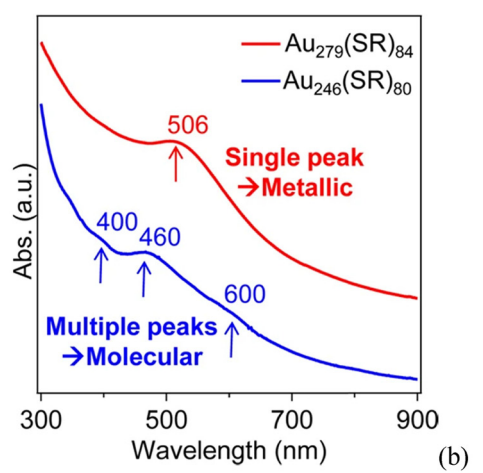


**Figure 2:** The sharp transition between nonmetallic and metallic electronic properties in atomically precise AuNCs spanning just 1.4–1.6 nm sizes. (a) The bandgap energy ( $E_{\rm g}$ ) is plotted against nanocluster diameter, displaying a clear transition from semiconducting behavior with a HOMO–LUMO gap (>0) for quantum-confined 1.4 nm Au246 to metallicity with a closed gap (= 0) emerging for slightly larger 1.6 nm Au279. (b) Optical absorption spectra reflect this dramatic change with distinct molecular excitations for Au246 evolving into an emergent continuum profile consistent with the metallic density of states for Au279. Copyright with permission from the study of Jin and Higaki [44].

evolution – non-metallic Au246 has distinct molecular excitations, while metallic Au279 starts exhibiting continuous excitation bands indicative of metallic density of electronic states. Figure 2a shows the transition in the energy bandgap ( $E_{\rm g}$ ) as a function of nanocluster size, going from a clear bandgap for non-metallic Au246 (contains 246 gold atoms, with a diameter of ~1.4 nm) to a closed gap demonstrating metallic behavior for Au279 (contains 279 gold atoms, with a larger diameter of ~1.6 nm). It displays a distinct HOMO–LUMO gap ( $E_{\rm g}$  > 0), indicating molecular, non-metallic properties. It shows a closed bandgap ( $E_{\rm g}$  = 0), signaling an emergence of metallicity. Thus, a clear transition from non-metal

to metal properties occurs over a minimal size range of 1.4–1.6 nm. Figure 2b shows the impact of this electronic structure transition on the optical absorption spectrum. Non-metallic Au246 displays distinct molecular excitations. Metallic Au279 starts showing an emergent continuum indicative of the metallic density of states. This demonstrates the dramatic change in properties across the sub-2 nm size range in GNPs as quantum confinement effects diminish and metallicity appears. As more gold atoms are added beyond Au279, the plasmon feature is expected to intensify further and progressively red shift to longer wavelengths. Therefore, while fully formed plasmons require larger (>3 nm) particles, the seeds of collective plasma oscillation first emerge around the Au246-Au279 nonmetal-tometal transition regime – marking the dawn of the nascent plasmon.

# 3 AuNCs in advanced energy storage: revolutionizing battery technologies

AuNCs have recently emerged as promising materials for advanced energy storage applications due to their unique structural, optical, electronic, and chemical properties. Composed of just a few to a hundred gold atoms and sizes under 2 nm, AuNCs exhibit molecular-like behaviors that differ fundamentally from the metallic properties of larger GNPs [42]. This enables precise control and tuning of AuNCs' properties by carefully tailoring size, composition, and surface chemistry during synthesis [45]. When effectively harnessed, these characteristics endow AuNCs with tremendous potential to enhance various electrochemical energy storage systems, including batteries, supercapacitors, and fuel cells. Their ultra-small size, high surface area, and biocompatibility further expand their potential for interfacing with biological systems for biomedical applications [46]. This article elucidates recent advances in integrating AuNCs into energy storage systems and devices while analyzing the underlying charge storage mechanisms and strategies to fully realize their promise from laboratory settings to practical implementation [47]. A predominant advantage of AuNCs for energy applications lies in their ultra-high surface area, which promotes increased reactivity and facilitates rapid electron and ion transport during energy storage [48]. For example, AuNC integration as electrode materials in Li-ion and Li-S batteries led to higher charge capacities and faster reaction kinetics attributed to amplified electrodeelectrolyte contact area. AuNCs' ready biocompatibility and

non-toxicity have also enabled their usage in biological settings for potential bioenergy applications, such as glucose fuel cells and neuro-electronic interfaces. Overall, AuNCs' high surface area enhances electrochemical performance. At the same time, their demonstrated biocompatibility in physiological environments expands their versatility across a wide breadth of advanced energy storage systems, spanning traditional electrochemical devices to futuristic biomedical systems. In addition, AuNCs exhibit intriguing luminescence properties based on quantum size effects, with emission tunability across the visible and near-infrared regions achievable by controlling size and composition. This enables their parallel use as sensory probes for tracking electrochemical processes in situ. Concurrently, the rich chemistry of gold facilitates straightforward AuNC functionalization with various ligands, polymers, biomolecules, and NPs. These multifaceted surface modification capabilities allow custom-tailoring of AuNCs' optical, electronic, stability, and solubility properties for integration into specific energy systems ranging from aqueous to non-aqueous environments. Overall, the integrated functionality of AuNCs' environment-sensitive fluorescence and versatile surface chemistry adds a multifunctional dimension to their energy applications. As predominant electrochemical energy storage systems, battery technologies stand poised for transformative advancements enabled by multifunctional AuNC incorporation targeting improvements across battery components – from electrodes to electrolytes to separators. Recent research has unveiled the intriguing interplay between AuNCs' unique quantum-derived properties and electrochemical charge storage processes spanning diverse battery chemistries. In particular, leveraging AuNCs as advanced battery electrode materials has demonstrated tremendous potential. As catalysts, AuNCs enhanced the kinetics of electrochemical reactions involved in the chargedischarge cycles in Li-ion, Li-S, and Zn-air batteries. This catalyzing ability boosted energy densities while improving cycle lifetime and stability – key metrics determining overall battery performance. Proposed mechanisms indicate AuNC catalysis facilitates redox reactions and mitigates intermediate byproduct accumulation on electrodes, which can deteriorate the battery function over extended cycles. AuNC integration helps batteries maintain higher energy conversion efficiencies over prolonged usage - a prerequisite for real-world implementation. Furthermore, AuNCs can uniquely mediate a battery's complex redox processes involving electron transfers between electrodes and electrolytes. For example, in Li-S batteries, AuNCs served dual catalytic roles – first in mediating polysulfide redox kinetics to curb the polysulfide shuttle effect, which leads to capacity fading, and second in electrocatalytically converting polysulfides to boost Coulombic efficiency correlating with

enhanced energy density metrics. These synergistic roles underscore how judiciously designed AuNCs can dually catalyze targeted battery reactions while converter unfavorable byproducts, culminating in better charge-discharge characteristics. Additionally, conductive AuNC integration improved reaction rates by increasing electrical conductivity within cathode composites. This strategy boosted power densities - another vital battery parameter governing rapid energy discharge capabilities. For example, conductive AuNC networks shortened ion diffusion pathways in supercapacitor electrodes, lowering equivalent series resistance and increasing power performance. Balancing trade-offs between energy density and power density remains an intrinsic material challenge. In this aspect, AuNCs have demonstrated preliminary success in concurrently improving both metrics – an encouraging indicator of their versatility for high-performance energy storage systems demanding high capacity and rapid power delivery. Progressing AuNC-based technologies from proof-of-concept to practical implementation requires elucidating the underlying nanoscale mechanisms governing their energy storage functionality. While initial studies have affirmed AuNCs' potential to enhance various electrochemical systems, recently concerted efforts have focused on theoretically and experimentally establishing an in-depth understanding of the structure-property interplay driving their charge storage dynamics. In particular, correlations between AuNC dimensions and resultant optical, electronic, and electrocatalytic properties form a key investigational avenue. For example, tighter quantum confinement induced with smaller AuNC sizes (sub-2 nm diameters) yielded higher fluorescence efficiencies. This permitted smaller AuNCs to operate as better real-time spectroscopic sensors of internal battery processes. Conversely, larger AuNC sizes near the quantum-tometallic transition threshold (~2-3 nm) offered higher electron densities, improving electrical conductivity and electrocatalytic performances. Overall, precise size tuning allows optimally harnessing AuNCs' size-dependent properties to best fit targeted battery applications. At the same time, a deeper understanding of quantum effects governing these phenomena aids deliberate design strategies. Furthermore, clarifying AuNCs' specific roles within the complex dynamics of battery charge storage mechanisms remains imperative. Recent studies have used spectroscopic monitoring and electrochemical testing methods to track AuNC participation across battery charge-discharge stages. The garnered insights explain experimental observations of AuNC-induced improvements in charge capacities, reaction rates, and stability. For example, quantifying AuNCs' precise contributions in catalyzing various redox reactions or electrostatically storing charge carriers sheds light on their battery functionality. These atomic-scale

perspectives of interfacial charge transfer processes facilitate the knowledge-driven design of AuNC structures to maximize energy storage capabilities.

# 3.1 Electrode enhancement: AuNCs as pioneering electrode materials

AuNCs are used as pioneering electrode materials, marking a transformative leap in advancing energy storage technologies. Through innovative design strategies, the geometric and electronic structures of AuNCs are tailored to enhance electrode performance, offering a high degree of design flexibility. This review comprehensively explores the impact of AuNC-based electrodes on various energy storage systems, ranging from Li-ion batteries to emerging technologies like Li-S and Zn-air batteries and supercapacitors. By delving into the underpinning mechanisms, the study elucidates the fundamental aspects contributing to the superior performance of AuNCs in energy storage applications. Additionally, the review addresses safety considerations associated with AuNC utilization. It highlights ethical dimensions, emphasizing responsible practices for the environmentally sustainable and ethical use of AuNCs in pursuing revolutionary advancements in energy storage technologies. Young et al. [49] discussed methods to attach small GNPs to electrodes through molecular linkers to improve electron transfer and increase the accessible surface area for electrochemical applications. Two approaches were developed: (1) directly grafting undecenethiolate-stabilized GNPs to boron-doped diamond electrodes through photochemical grafting of the NP ligand shell and (2) assembling triphenylphosphine-stabilized GNPs onto undecyl thioacetate molecular monolayers covalently bound to the electrode surface through ligand exchange. GNPs retained their size and composition after being attached to the electrodes through either method. Electrochemical studies using a ferrocene redox probe attached to the NP surfaces showed that the molecularly tethered NPs exhibited more efficient electron transfer and higher electrochemically active surface area than NPs deposited by solution methods. The results demonstrate that defining the NP-electrode interface through molecular linkers can significantly improve the electrochemical properties of NP-functionalized electrodes. Im et al. [50] discussed an GNP ink formulation for the additive manufacturing of electronic components. The authors introduced a multifunctional thiol called trimethylolpropane tri(3-mercapto propionate) or TrisSH as a cohesion enhancer in the ink to prevent cracks and pores from forming. TrisSH binds to the surface of neighboring GNPs through its thiol

groups, improving the cohesion between the particles. The inkjet-printed gold electrode with TrisSH shows an electrical conductivity of 3.0 × 106 S/m and remains stable under repeated mechanical deformation and in phosphate-buffered saline solution. The presence of TrisSH helps form more uniform layers with lower porosity during sintering, resulting in reduced organic ligands and enabling conductive channels between NPs. This gold ink with enhanced cohesion shows potential for flexible printed electronics and bioelectronic applications. Figure 3 provides a comprehensive overview of the synthesis, characterization, and ink formulation of octane thiol-functionalized GNPs (OT-GNPs) for inkjet printing applications. The schematic in Figure 3a outlines the synthesis of OT-GNPs and the ink formulation, incorporating a multifunctional thiol (TrisSH) as a cohesion enhancer. Transmission electron microscopy (TEM) images in Figure 3b illustrate the morphology of OT-GNPs, showcasing their core diameter and distribution. The ink formulation process is captured in Figure 3c, featuring photographs of two ink formulations, Au-TrisSH and Ctrl-Au, with and without TrisSH. The inkiet deposition of the Au-TrisSH ink is schematically represented, accompanied by a photograph of an inkjet-printed gold square-planar spiral coil. The dependence of line widths on drop spacing (DS) values is depicted in Figure 3d, including an optical microscopy image of GNP lines printed at different DS values. Finally, Figure 3e delves into the electrical resistivity of printed Ctrl-Au and Au-TrisSH lines at varying sintering temperatures, supported by optical microscopy images of post-treated lines at  $T_{\text{sint}}$  = 150°C. The figure provides a comprehensive visual representation of the synthesis and application of OT-GNPs in inkjet printing technology.

## 3.2 Boosting battery performance with **AuNC** electrodes

Integrating AuNCs into electrode materials addresses key challenges that traditional battery technologies face [47]. Their high surface area facilitates improved reactivity and allows for efficient charge and ion transport, resulting in enhanced electrochemical performance [51]. Researchers are actively exploring the potential of AuNCs in different battery systems, including lithium-ion batteries, lithiumsulfur batteries, and other emerging energy storage technologies [52]. The ability to tailor the properties of AuNCs further contributes to their versatility, enabling the design of electrodes with specific characteristics to meet the

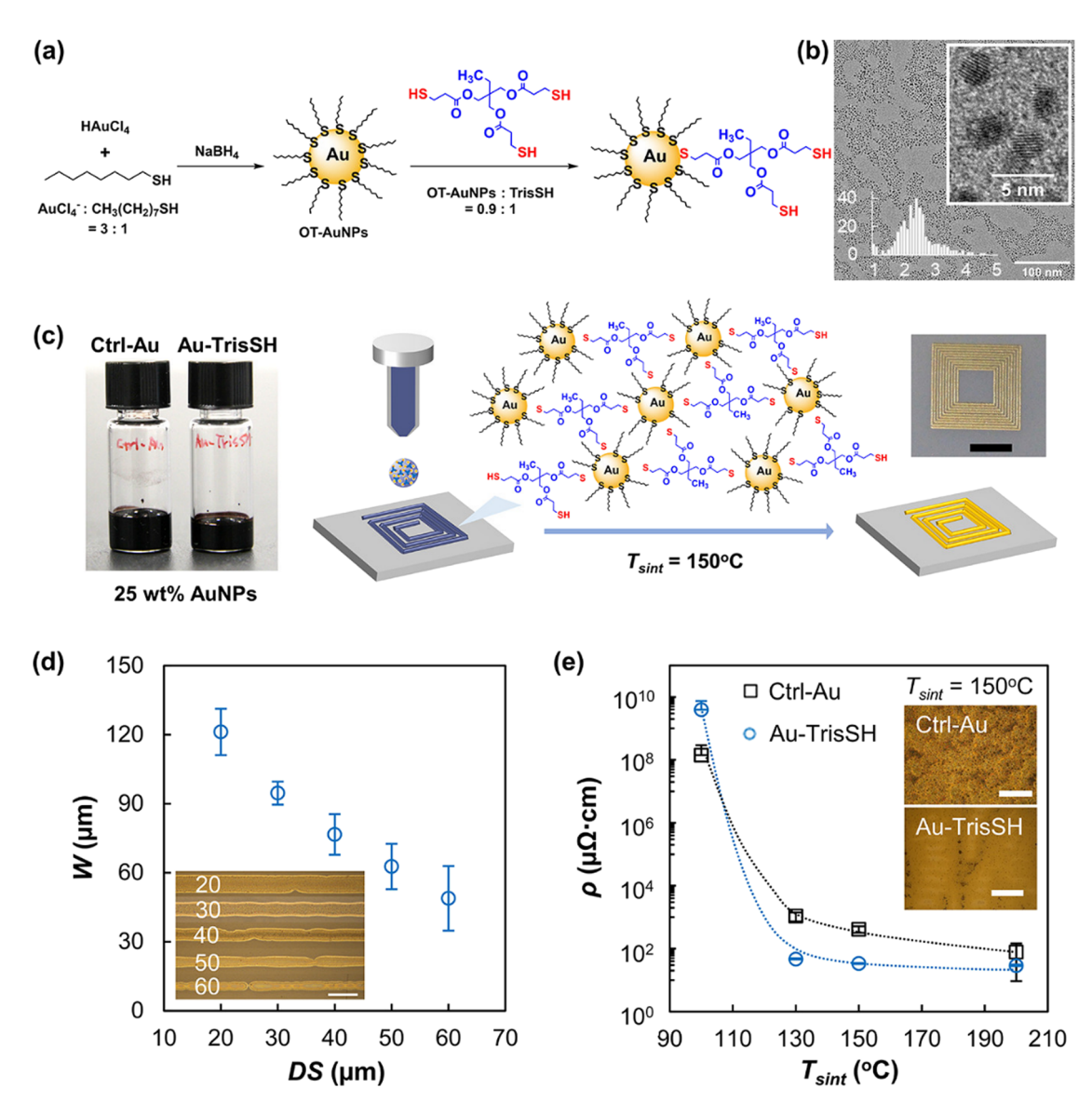


**Figure 3:** Multi-faceted aspects of synthesizing and utilizing octanethiol-functionalized GNPs (OT-GNPs) for inkjet printing applications. (a) Schematic representation provides insights into the synthesis process of OT-GNPs and the subsequent ink formulation, incorporating a multifunctional thiol (TrisSH) for enhanced cohesion. (b) High-resolution transmission electron microscopy (HRTEM) images offer a detailed view of OT-GNPs, showcasing their morphology, with a histogram presenting the size distribution. (c) a photograph displays two ink formulations, Au-TrisSH and Ctrl-Au, with and without TrisSH, along with a schematic of the inkjet deposition process and an inset photograph of an inkjet-printed gold square-planar spiral coil. (d) Dependence of line widths on DS values, featuring an optical microscopy image of GNP lines printed at different DS values. (e) Electrical resistivity of printed Ctrl-Au and Au-TrisSH lines at varying sintering temperatures, complemented by optical microscopy images of post-treated lines at  $T_{\text{sint}}$  = 150°C. The dotted lines in the insets serve as guides, enhancing the clarity of the presented data. Overall, Figure 1 encapsulates the synthesis, characterization, and application of OT-GNPs in inkjet printing processes.

demands of diverse applications [42]. AuNC electrodes exhibit notable advantages in lithium-ion batteries. The ultra-small size of AuNCs facilitates better intercalation of lithium ions, leading to increased charge and discharge rates. The precise control over composition enables researchers to fine-tune the electrochemical properties of AuNC electrodes, optimizing their performance in lithium-ion battery systems. Additionally, the high surface area of AuNCs enhances the

overall capacity and efficiency of lithium-ion batteries, making them attractive candidates for next-generation energy storage solutions. Lithium–sulfur batteries, known for their high theoretical energy density, face challenges related to polysulfide shuttling and low cycle life. AuNC electrodes offer a promising solution by serving as efficient catalysts for anchoring and rapidly converting lithium polysulfides (LiPS). This capability significantly mitigates the polysulfide shuttle effect, improving

cycling stability and prolonged battery life. Integrating AuNCs with graphene nanosheets further enhances the structural integrity of the battery separator, contributing to the overall success of lithium-sulfur battery systems. The benefits of AuNC electrodes extend beyond conventional battery technologies. Researchers are exploring their application in other emerging energy storage systems, including supercapacitors and beyond. The remarkable properties of AuNCs position them as versatile and multifunctional materials for addressing the evolving challenges in the field of energy storage. Despite the tremendous progress, several challenges and opportunities lie ahead in utilizing AuNC electrodes for energy storage [53]. Further research is needed to explore the long-term stability, scalability, and cost-effectiveness of AuNC-based electrode materials. Additionally, efforts to understand the underlying mechanisms of AuNC-enhanced battery performance will contribute to the rational design of electrode materials for specific applications. Shen et al. [54] developed an aptamerbased impedimetric biosensor for detecting the allergen Der p2 from dust mites. The biosensor uses aptamers instead of antibodies to recognize the target allergen. The researchers first created an anodic aluminum oxide membrane with a nanohemisphere array surface. This was used as a template to electroform a nickel nanomold with a concave nanostructure. The nickel mold was then used to replicate a nanostructured polycarbonate (PC) substrate via hot embossing. Finally, a thin gold film was sputtered onto the PC to create a double-generation GNP electrode. Specific aptamers for Der p2 were selected using a magnetic-assisted rapid aptamer selection method. The aptamers were then immobilized on the electrode surface. Electrochemical impedance spectroscopy was used to measure the resistance change upon binding different Der p2 concentrations. The biosensor showed a sensitivity of 2.088  $\Omega/(ng/mL \times cm^2)$ , a dynamic detection range of 27.5–400 ng/mL, and a detection limit of 16.47 ng/mL for Der p2. Compared to conventional antibodybased sensors, the aptamer-based biosensor has advantages such as ease of synthesis, high purity, and high controllability of the aptamers. Figure 4 depicts a schematic of a

double-generation GNPs electrode. The fabrication process involves several sequential steps. First, an anodic aluminum oxide (AAO) membrane is prepared. Next, the surface of the AAO barrier layer is modified. Subsequently, a nanostructured nickel mold is fabricated. The nanostructured PC substrate is then created through replica molding using the nickel mold. After that, a thin layer of gold is sputtered onto the PC substrate. Finally, the electrode is packaged. This fabrication aims to create a specialized electrode with GNPs for use in various applications such as energy storage or catalysis. Figure 5(a) and (b) display scanning electron microscope (SEM) images of the electrodes produced with different sputtering conditions. Figure 5(a) demonstrates that applying a current of 30 mA for 150 s results in the formation of double-generation GNP electrodes with uniformly distributed gold nanoparticles (GNPs), showcasing a size distribution of 29-40 nm. On the other hand, Figure 5(b) reveals that a longer sputtering time of 180 s only deposits a thin gold film without distinct NPs.

Subsequently, Figure 5(c) and (d) depict SEM images of the 30 mA, 150 s sputtered gold electrode subjected to annealing at temperatures of 100 and 130°C, respectively. To maintain the integrity of the PC substrate, the annealing temperature is kept below the glass transition temperature of PC (145°C). Figure 3(d) illustrates that under annealing at 130°C, the GNPs on the nano hemispheres melted, resulting in a smooth thin film. Therefore, the optimal conditions for fabricating double-generation GNP electrodes involve sputtering with an applied current of 30 mA for 150 s, followed by annealing at 100°C, as depicted in Figure 5(c).

# 3.3 Applications in emerging battery technologies (e.g., Li-S, Zn-air)

Fadeev *et al.* [55] outlined the simple two-step synthesis method as an effective way to produce iron oxide@gold NPs with promising properties for use as anode materials

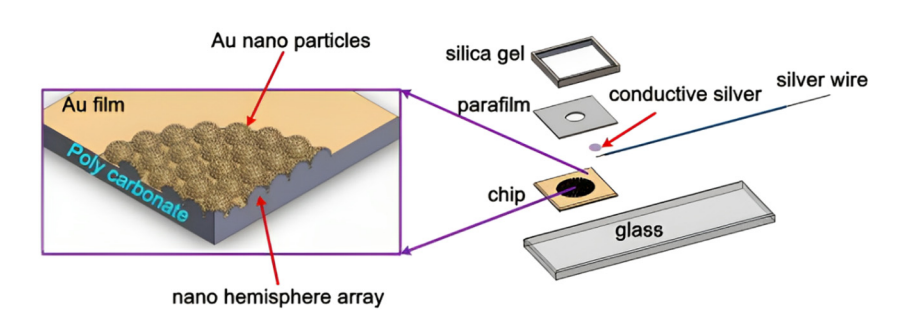
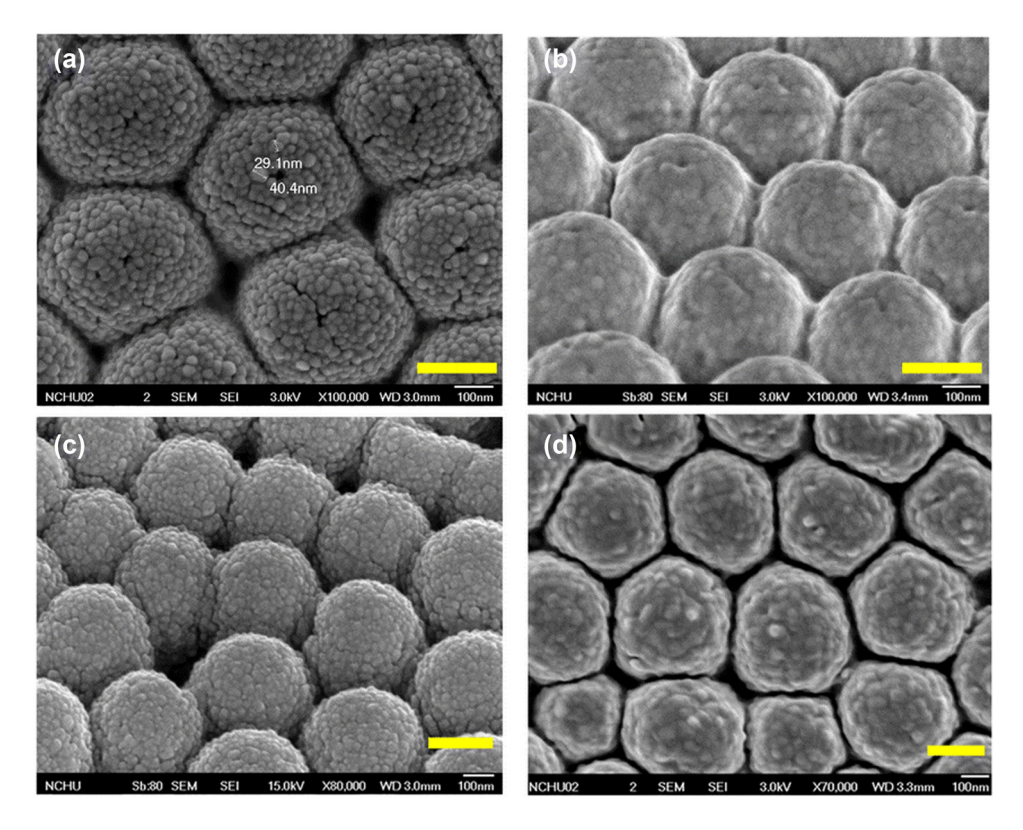


Figure 4: Schematic of the proposed double-generation GNP electrode.



**Figure 5:** SEM images illustrating the characteristics of the double-generation GNP electrode under different fabrication and annealing conditions. (a) The electrode is obtained by applying a sputtering current of 30 mA for a duration of 150 s. This results in uniformly distributed GNPs with a size distribution of 29–40 nm. In contrast, (b) shows the result of a longer sputtering duration of 180 s, which only forms a thin gold film without distinct NPs. Subsequent annealing at different temperatures is depicted in (c) and (d). In (c), the electrode is subjected to further annealing at 100°C, maintaining the integrity of the PC substrate. However, in (d), annealing at a higher temperature of 130°C causes the GNPs on the nano hemispheres to melt, resulting in a smooth thin film. The optimal conditions for the fabrication involve sputtering with a current of 30 mA for 150 s, followed by annealing at 100°C, as demonstrated in (c). Copyright and permission from the study of Shen *et al.* [54].

in lithium-ion batteries. The researchers synthesized iron oxide NPs using a co-precipitation method and then coated them with gold to form iron oxide@gold core-shell NPs. Various techniques such as XRD, SEM, TEM, LDA, and Mössbauer spectroscopy were used to characterize the NPs and confirm the core-shell structure. The gold coating converted almost all the iron oxide core to maghemite and stabilized the NPs. Electrochemical tests show that the iron oxide@gold NPs can potentially be used as anode materials for lithium-ion batteries. They exhibited a capacity of up to 1,380 mA h/g and good rate performance. Compared to lithium-ion batteries, sulfur has a higher theoretical capacity [56]. However, several issues prevent their commercialization. The main problem is the polysulfide shuttle effect caused by the dissolution of LiPS intermediates in the electrolyte. This leads to capacity fading and loss of active material. Other issues include sulfur's poor electrical conductivity, volume expansion of sulfur during charging and discharging, and safety concerns with the lithium metal anode. Several approaches have been explored to address

these issues. Nanofabrication of the sulfur cathode with conductive carbon hosts can improve sulfur utilization and trap polysulfides. Using polar polysulfide adsorptive materials like metal oxides and polymers in the cathode and separator can help anchor polysulfides. Solid electrolytes and alternative anode and cathode materials like lithium sulfide and silicon can suppress the polysulfide shuttle effect [57]. For lithium–sulfur batteries to be commercially viable, researchers need to focus on improving conductivity, pore volume, polysulfide adsorption, cycle life, capacity retention, and safety while making the synthesis methods scalable and cost-effective [58]. Overcoming these challenges could enable lithium–sulfur batteries to provide higher energy density at a lower cost than lithiumion batteries.

Sun *et al.* [59] demonstrated that metal nanoclusters like Au<sub>24</sub>Pt (phenylethanethiolate)<sub>18</sub> have the potential as optimal electrocatalysts for lithium–sulfur batteries to improve their performance. Specifically, Au<sub>24</sub>Pt(PET)<sub>18</sub> nanoclusters were studied for their ability to anchor and convert LiPS species in

lithium-sulfur batteries. Metal nanoclusters have unique properties that make them promising as catalysts, but their application as practical electrocatalysts remains unexplored mainly [60]. Au24Pt(PET)18 nanoclusters were found to have multiple active sites that could effectively bind soluble LiPS and catalyze their conversion to insoluble lithium sulfides. An Au24Pt(PET)18@graphene composite modified separator was prepared and used in lithium-sulfur batteries. It demonstrated a high reversible capacity of 1535.4 mA h/g at 0.2 A/g and a rate capability of 887 mA h/g at 5 A/g. The batteries also showed long cycling stability, retaining 558.5 mA h/g capacity after 1,000 cycles at 5 A/g and a low-capacity fading rate of 0.041% per cycle. The Au24Pt(PET)18 nanoclusters were found to promote the sulfur redox kinetics and reduce the energy barrier for the rate-limiting step in the sulfur reduction reaction. The microstructure characterization of the battery separator involving Au24Pt(PET)18@G nanosheets was conducted through SEM and TEM. The cross-sectional SEM view illustrated that the Au24Pt(PET)18@G and polypropylene (PP) layers had thicknesses of 23.20 and 21.32 µm, respectively (Figure 6a). The graphene surface appeared smooth, as shown in Figure 6b, with metal nanoclusters exhibiting even dispersion and minimal agglomeration. Figure 6c-e further confirmed the uniform distribution of metal nanoclusters on the graphene surface. The intense ultrasound treatment during TEM sample preparation validated the composite's stability. This homogeneous dispersion of metal nanoclusters on graphene not only provided abundant active sites for immobilizing polysulfide species and accelerating redox reactions but also reduced local current density and volume changes, forming a buffer layer on the lithium surface to stabilize the lithium anode and inhibit dendrite formation. The selected area electron diffraction (SAED) pattern (Figure 6f) displayed multidiffraction rings corresponding to Au and Pt crystal faces, and the magnified view with fast Fourier transform (FFT) patterns (Figure 6g and h) confirmed the lattice spacing of 0.246 nm attributed to Au(111) planes (Figure 6i). Elemental mapping using energy-dispersive X-ray spectroscopy (EDX) illustrated the uniform distribution of elements within the Au24Pt(PET) 18@G composite (Figure 6j-m). This detailed microstructural analysis underscores the well-dispersed and stable nature of the metal nanoclusters on the graphene surface, showcasing their potential for enhanced electrocatalytic performance in lithium-sulfur batteries.

The Au24Pt(PET)18 nanoclusters strategically play a pivotal role in synergistic adsorption and catalytic conversion of LiPS intermediates, thereby contributing to the advancement of high-energy-density and long-life lithiumsulfur batteries (LSBs), as depicted in Figure 7. The even distribution of Au24Pt(PET)18 clusters on graphene sheets

serves as catalytic sites, effectively anchoring soluble longchain LiPSs and facilitating their conversion to insoluble short-chain Li2S2/Li2S. Simultaneously, graphene enhances electron/ion transport within the battery system. The LSBs constructed with the Au24Pt(PET)18@G-based separator showcase remarkable performance by mitigating the shuttling of polysulfides, preventing the formation of lithium dendrites, and improving sulfur utilization. This innovative approach demonstrates superior capacity and cycling stability, underlining the significant contribution of the Au24Pt (PET)18 nanoclusters in optimizing the performance of LSBs.

Marangon et al. [61] doped sulfur with a few GNPs is an effective way to develop high-performance lithiumsulfur battery cathodes with high sulfur loading, high capacity, and good cycling stability. The authors prepared a composite of 97% sulfur and 3% GNPs by mixing molten sulfur with GNPs. They characterized the composite using X-ray CT, electron microscopy, and X-ray diffraction techniques. The gold-doped sulfur composite cathode shows highrate capability, maximum capacity over 1,300 m Ah g S<sup>-1</sup>, and capacity retention of 85-91% after 100 cycles at high rates. X-ray CT analysis reveals that the GNPs help enhance sulfur conversion kinetics and improve cell performance. The GNPs form micro and sub-micro aggregates that increase the electronic conductivity of the sulfur electrode, enable high sulfur loading, and act as catalysts for polysulfide conversion. The gold-doped sulfur composite electrode achieves a high areal capacity of 5.4 mAh cm<sup>-2</sup> with an electrolyte-tosulfur ratio of 5 μL mg<sup>-1</sup> and an active material loading of  $5.7 \text{ mg cm}^{-2}$ .

Zhu et al. [62] developed a method to produce strained palladium-gold Janus NPs that show enhanced electrocatalytic performance for oxygen reduction and potential use in zinc-air batteries. The tensile strain was found to lower the energy barrier for the rate-determining step of oxygen reduction, improving the catalyst activity. The researchers synthesized palladium-GNPs supported on graphene oxide through a two-step process. GNPs were first grown on silicon nanowires, and then palladium NPs were grown epitaxially on the gold. This produced a Janus NP structure with palladium under tensile strain up to +4%. The palladium-GNPs showed better ORR performance than commercial platinum catalysts in an alkaline medium. The tensile strain gave the catalyst a higher half-wave potential and mass activity. When used as the cathode catalyst for a zinc-air battery, the palladium-GNPs exhibited a high peak power density and good long-term durability.

Nguyen et al. [63] proposed a new hybrid material called Au@Co2N0.67/3D-NGr for efficient water splitting and zinc-air batteries. The Au@Co2N0.67/3D-NGr hybrid comprises Au@Co2N0.67 core-shell nanodots anchored

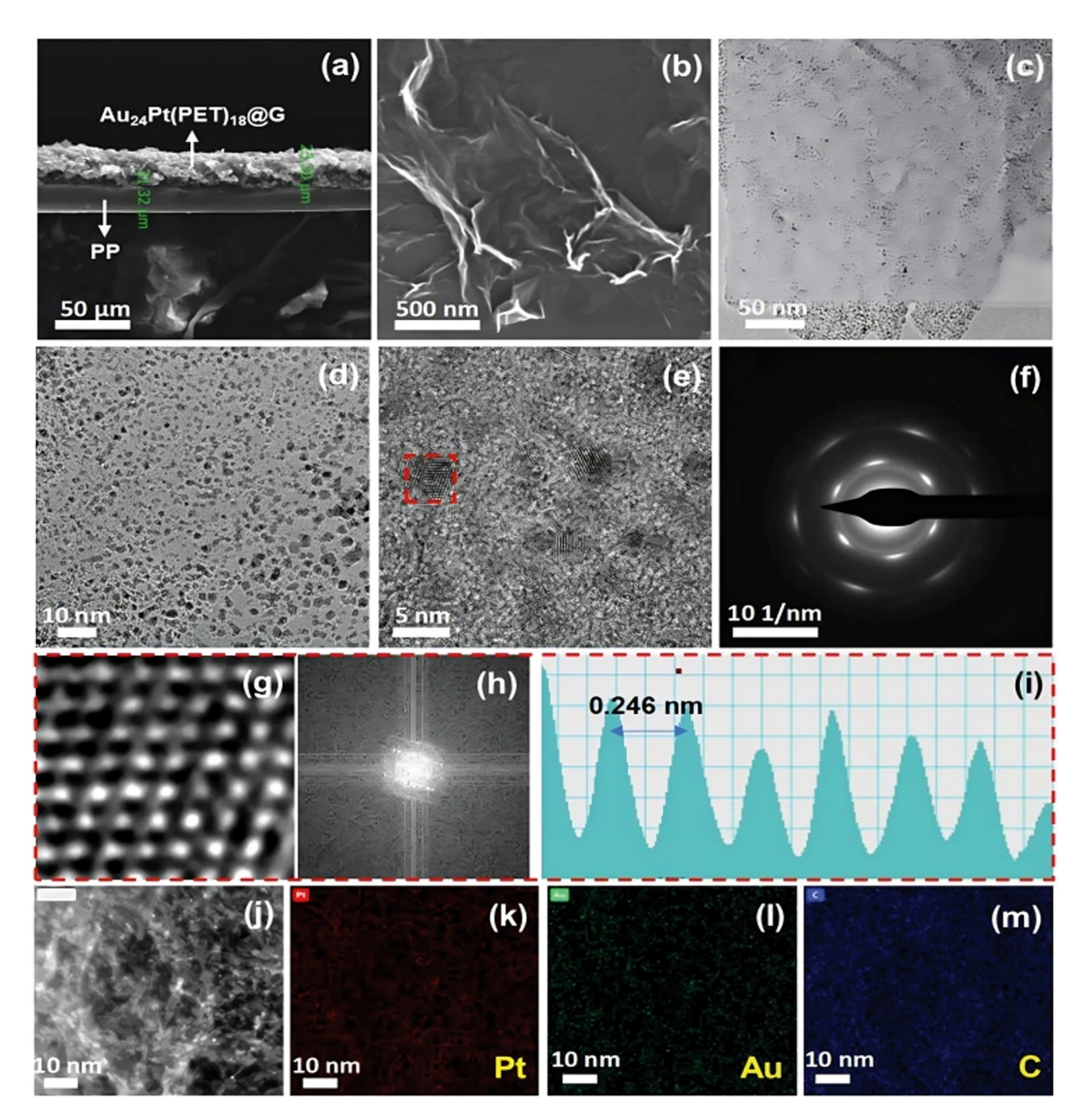


**Figure 6:** A detailed insight into the microstructure of the Au24Pt(PET)18@G composite, highlighting its well-dispersed metal nanoclusters on the graphene surface and confirming their stability and crystalline nature. (a) The SEM cross-sectional view of the Au24Pt(PET)18@G/PP separator depicts the layered structure with thickness measurements for Au24Pt(PET)18@G and PP layers. (b) SEM image of the graphene surface with evenly dispersed metal nanoclusters, highlighting the smooth morphology. (c)–(e) TEM images reveal the uniform distribution of Au24Pt(PET)18 nanoclusters on the graphene surface, demonstrating their well-dispersed nature. (f) The SAED pattern exhibits multi-diffraction rings assigned to Au and Pt crystal faces, confirming the crystalline structure of the metal nanoclusters. (g) Magnified view of the region marked by the red rectangle in (e), providing a closer look at the arrangement of metal nanoclusters on graphene. (h) FFT pattern corresponding to the red rectangle in (e), further emphasizing the crystallographic information. (i) Distance *versus* intensity plot from the red rectangular section in (e), indicating the lattice spacing of 0.246 nm attributed to Au(111) planes. (j) TEM image displaying the overall structure of the Au24Pt(PET)18@G composite. (k)–(m) Elemental maps for Pt, Au, and C, respectively, showing the uniform distribution of these elements in the composite. Copyright with permission from the study of Sun *et al.* [59].

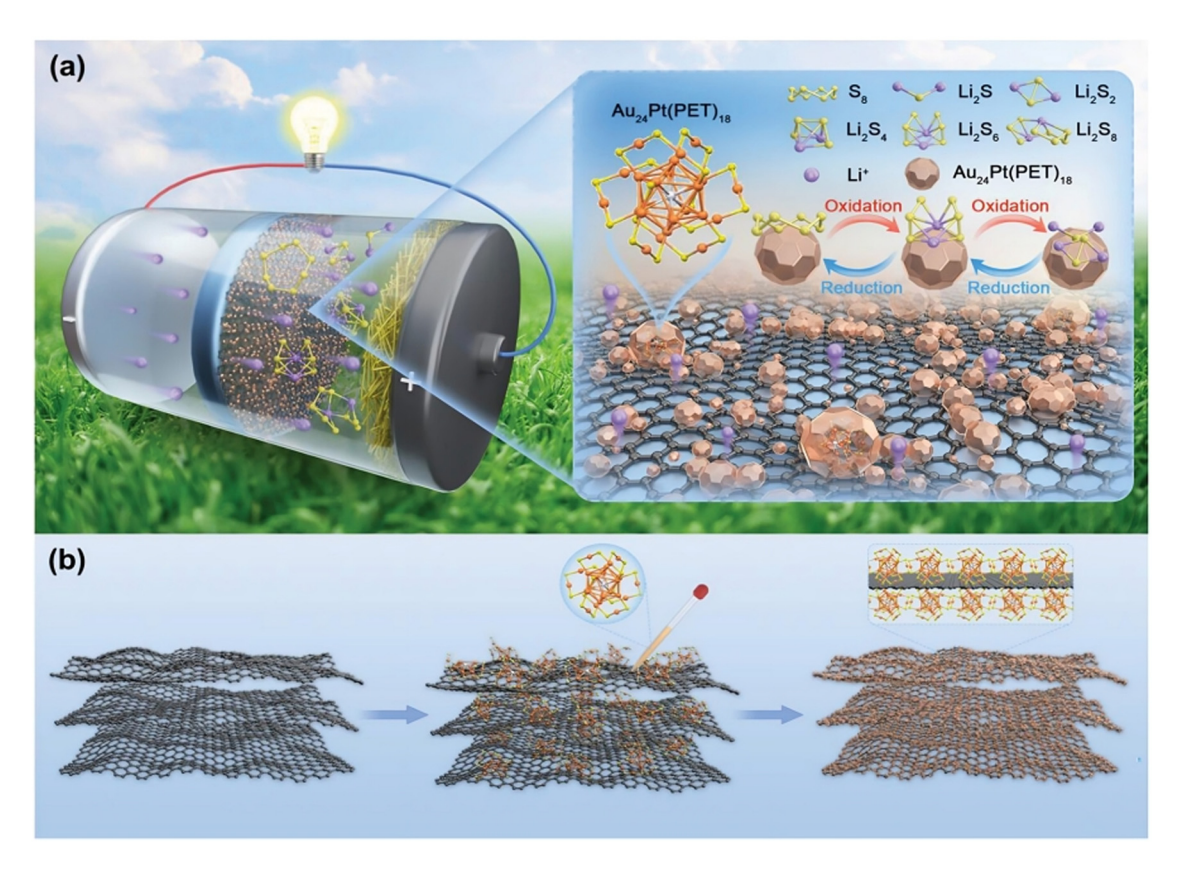


**Figure 7:** (a) Li–S battery incorporating an Au24Pt(PET)18@G-modified separator designed for the adsorption of LiPS. The catalytic properties of the Au24Pt(PET)18 nanoclusters facilitate the reduction of elemental sulfur (S8) to LiPSs and the subsequent conversion to insoluble Li2S2/Li2S. Additionally, the nanoclusters play a role in oxidizing Li2S/Li2S2 back to LiPSs and S8. This synergistic adsorption and catalytic conversion mechanism enhances the battery's overall performance by minimizing polysulfide shuttling and optimizing sulfur utilization. (b) The preparation process depicts the synthesis of Au24Pt(PET)18@G nanosheets, highlighting the strategic combination of graphene and Au24Pt(PET)18 nanoclusters to form the modified separator. Copyright with permission from the study of Sun *et al.* [59].

on 3D interconnected nitrogen-doped graphene hollow microspheres. The Au core is a "promoter" that activates the electrocatalytic activity of the Co2N0.67 shell by modulating its electronic structure through their interface interaction. The 3D-NGr is an ideal support to prevent aggregation of the Au@Co2N0.67 nanodots and provide a pathway for electron and mass transport. Synergistic effects between the Au@Co2N0.67 nanodots and 3D-NGr substrate can enhance the number and types of active sites and optimize adsorption/desorption for multi-electrochemical reactions. The Au@Co2N0.67/3D-NGr hybrid catalyzes the hydrogen evolution reaction (HER), oxygen evolution reaction (OER), and ORR simultaneously with small onset potential, overpotential, and low Tafel slopes. The assembled water electrolyzer based on Au@Co2N0.67/3D-NGr shows excellent performance and stability. Zinc-air batteries using this hybrid also demonstrate high performance and good stability.

# 4 Catalytic hydrogenation: GNPs as catalysts for hydrogen storage

Hydrogen (H<sub>2</sub>) is recognized as a promising and eco-friendly energy source, positioning itself as a leading contender to replace conventional fossil fuels. Among the various methods for hydrogen production, the photocatalytic water-splitting system stands out for its simplicity and cost-effectiveness, representing an ideal approach to harnessing solar energy for hydrogen fuel generation directly. This system integrates photoanode and photocathode materials in a powdered form, allowing for water-splitting reactions using pure solar energy without needing an external circuit. Numerous configurations of photocatalysts have emerged, emphasizing the importance of high-efficiency photocatalysts with tunable features such as morphology, structure, composition, and element ratio. Semiconductor materials, widely employed as basic photocatalysts, generate high-energy charge carriers when

excited by solar light. These carriers then separate, with electrons and holes migrating to catalytically active sites, driving chemical transformations for hydrogen and oxygen evolution half-reactions. Plasmonic metals like Au, Ag, Cu, and Al enhance light absorption efficiency and are often integrated with semiconductors for efficient photocatalytic water reduction and oxidation processes [64]. Oshikiri et al. [65] demonstrated that modal strong coupling between plasmons and nanocavities can enhance hot-carrier injection and HER on photocathodes under visible light. The research article discusses a novel photocathode developed for boosting hydrogen evolution under visible light wavelengths. The photocathode combines GNPs, lithiumdoped nickel oxide, and a platinum film (Figure 8). Figure 8 displays a groundbreaking approach to photocatalysis, utilizing a photocathode comprising GNPs, p-type nickel oxide, and a platinum film. Operating under modal strong coupling conditions, this innovative design enables the absorption of visible light across a broad wavelength spectrum (500-850 nm), offering unprecedented potential for efficient hydrogen evolution. (I) Understanding modal strong coupling: Delves into modal strong coupling and its implications in photocathode design. How hybrid modes, facilitated by strong modal coupling, contribute to enhanced light absorption and energy transfer within the photocathode structure are explored. (II) Wavelength range expansion: This highlights the significance of achieving hybrid modes over an extended wavelength range (500-850 nm). The advantages of broad-spectrum light absorption and its impact on boosting the efficiency of the photocatalytic process are discussed. (III) Photocathode components and operation consists of (a) GNPs: The role of GNPs in the photocathode structure is examined. Their contributions to light absorption, surface plasmon resonance (SPR), and the initiation of hot-hole injection into the p-type nickel oxide are investigated, which is crucial for the subsequent hydrogen evolution process. (b) P-type nickel oxide: The characteristics of p-type nickel oxide as a critical component in the photocathode are explored, and its role in facilitating efficient charge separation and transport is elaborated, which is crucial for the overall photocatalytic activity. (c) Platinum film: The significance of the platinum film in promoting hydrogen evolution is discussed. How platinum contributes to catalyzing water reduction by hot electrons generated through the photocatalytic process is analyzed. The GNPs act as plasmonic metals, the lithium-doped nickel oxide acts as a p-type semiconductor, and the platinum film acts as a reflection layer [66]. The nickel oxide on platinum film acts as a Fabry-Pérot nanocavity that absorbs visible light from 500 to 850 nm through hybrid modes formed by coupling between localized surface plasmon resonance (LSPR) of GNPs and the nanocavity modes [65]. This coupling or

"modal strong coupling" between the plasmon resonance and nanocavity modes enhances light absorption and promotes hot-hole injection from GNPs into nickel oxide [65]. The hot electrons then reduce substances like water or protons to evolve hydrogen gas. The fabricated photocathode showed a hydrogen evolution rate of 23 nanomoles per centimeter squared per hour under visible light irradiation, with a faradaic efficiency of around 70% for hydrogen evolution after 9 h.

In the photoanode, utilizing a combination of a metal and an n-type semiconductor, a reduction is constrained by the band structure of the semiconductor as electrons are injected into its conduction band. The additional energy from the LSPR used for hot-electron excitation is lost in this process (Figure 8b). In contrast, the photocathode, composed of a plasmonic metal and a hole-trapping material, efficiently induces reduction. Here, hot electrons reduce substances, involving hot-hole injection from the metal to the hole-trapping material (Figure 8c). Notably, Atwater *et al.* have reported that hot-hole injection from gold to a p-type semiconductor is thermodynamically preferable to hot-electron injection from gold to an n-type semiconductor, attributed to the energy distribution of hot carriers generated in gold, as estimated by theoretical calculations.

# 4.1 Enhanced catalytic activity in hydrogenation reactions

Hydrogenation reactions, which involve the addition of hydrogen to unsaturated compounds, are crucial in various industries, including petrochemicals, pharmaceuticals, and food production [67]. Achieving high catalytic activity in hydrogenation reactions is essential for improving reaction efficiency and selectivity. One effective strategy to enhance catalytic activity is the utilization of advanced catalysts, particularly those based on noble metals like GNPs. GNPs exhibit unique catalytic properties attributed to their size, morphology, and surface properties. The high surface area of GNPs provides abundant active sites, while their tunable electronic structure allows for precise control over catalytic behavior.

Additionally, the plasmonic properties of GNPs can enhance light absorption, promoting photocatalytic hydrogenation under illumination. Combining these features makes GNPs promising candidates for achieving enhanced catalytic activity in hydrogenation reactions. Researchers continue to explore innovative approaches and design principles to optimize GNP-based catalysts, contributing to the advancement of efficient and sustainable hydrogenation processes.

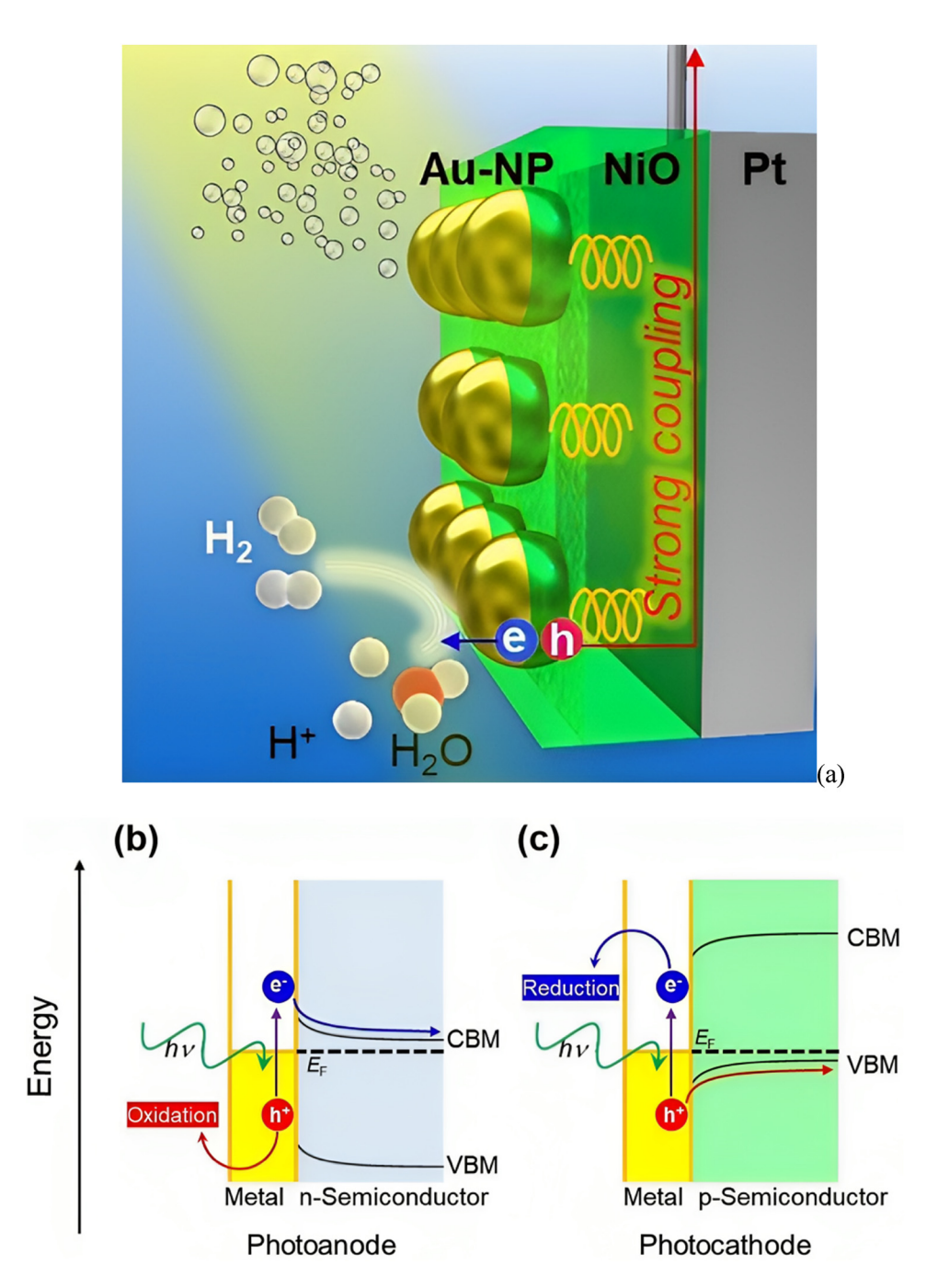


**Figure 8:** (a) The development of a high-performance photocathode, a synergistic structure designed by incorporating GNPs, p-type nickel oxide, and a platinum film under modal strong coupling conditions. This innovative photocathode exhibited remarkable light absorption properties across a wide wavelength range, specifically from 500 to 850 nm, leveraging hybrid modes facilitated by modal strong coupling. The key feature of this design was its ability to enhance hydrogen evolution through water reduction by utilizing hot-electron processes. Notably, this involved the efficient injection of hot holes from GNPs to nickel oxide, showcasing the potential of modal strong coupling to improve photocatalytic processes for hydrogen generation significantly. (b) Hot-electron injection at the interface of a plasmonic metal and an p-type semiconductor. CBM, VBM, and EF indicate the conduction band minimum, valence band maximum, and Fermi level, respectively. Copyright with permission from the study of Oshikiri *et al.* [65].

Titanium dioxide ( $TiO_2$ ) is a widely used semiconductor in hydrogen generation due to its low cost, excellent stability, and abundant availability on a large scale. However, its

limitation lies in predominantly absorbing UV light, given its large bandgap of 3.20 eV, which restricts its spectral response in the visible region. To address this, combining plasmonic NPs with visible-light responsiveness and semiconductive metal oxides like TiO<sub>2</sub> presents an opportunity to harness more solar light. Plasmonic absorption becomes crucial for generating high-energy hot electrons in the plasmonic NPs, facilitating efficient injection into the conduction band of TiO<sub>2</sub> [68]. Moreover, the strong localized electric field established at the interface between plasmonic NPs and TiO<sub>2</sub> promotes the separation of electron-hole pairs, facilitating the water-splitting process. Nguyen et al. [69] demonstrated this by placing porous Au NPs on highly ordered TiO<sub>2</sub> nanotube arrays, achieving controllable metal distribution and cocatalyst amounts. The resulting porous Au/TiO2 assemblies exhibited a fourfold increase in hydrogen production compared to normal Au/TiO<sub>2</sub>, attributed to optimized interface contact between porous Au NPs (active sites) and reactants. The integration of porous Au/ TiO<sub>2</sub> assemblies has demonstrated a significant fourfold increase in hydrogen production compared to normal Au/ TiO<sub>2</sub>, emphasizing the optimized interface contact between porous Au NPs and reactants. Zhang et al. [70] innovatively designed Janus Au multimer-TiO<sub>2</sub> nanostructures, leveraging whispering gallery mode (WGM) resonances for enhanced plasmonic photocatalysis. These resonances broadened the spectral range of hybrid photocatalysts, leading to substantially higher hydrogen evolution activity under visible-nearinfrared light compared to Au NPs, pure TiO<sub>2</sub> spheres, and Au@TiO2 core-shell structures. Various factors, including size, semiconductor type, energy band positions, plasmonic metal types, nanostructure morphology, and metal loading, play crucial roles in influencing photocatalytic reactions. For instance, combining CdSe quantum dots with Au NPs in Au/ CdSe nanocrystal clusters resulted in a remarkable tenfold increase in hydrogen evolution compared to pure CdSe NCs. This underscores the importance of plasmonic effects in promoting hydrogen evolution, aligning with the absorption spectrum of Au NPs. Researchers also highlight the significance of fabricating complex semiconductor systems to enhance light trapping, reduce charge recombination, and achieve suitable band edge potentials for efficient photocatalysis.

In the pursuit of optimizing photocatalytic systems, researchers explore the adjustment of structural morphology as a viable strategy. An illustrative example is the work by Mubeen  $et\ al.$ , who developed a plasmonic absorber incorporating Au nanorods (NRs), TiO<sub>2</sub>, and Pt NPs to serve as a hot carrier generator, hot electron filter, and H<sub>2</sub> evolution catalyst, respectively. The spectral irradiance significantly influenced the H<sub>2</sub> release rate in each device module, with varied aspect ratios of Au NRs. The "panchromatic" device, stacking Au NRs with aspect ratios of 1.4 and 3.0, demonstrated the ability to cover a substantial

portion of the solar spectrum, achieving a remarkable  $\rm H_2$  production of 2.3 µmol  $\rm h^{-1}$ . This production level surpassed that of devices utilizing Au NRs with a single aspect ratio of 1.4 or 3.0 by 1.8 or 3.5 times, emphasizing the impact of structural morphology adjustments on enhancing overall photocatalytic performance [71].

In a study by Ha et al. [72], Au/Cu2FeSnS4 (CITS) core-shell nanostructures were designed with various shapes of Au spheres and Au multipods as cores. The photocatalytic hydrogen evolution rate of Au multipod/CITS (0.09 µmol  $mg^{-1} h^{-1}$ ) exceeded that of pure CITS (0.0264 µmol  $mg^{-1} h^{-1}$ ) and Au sphere/CITS (0.0595 µmol mg<sup>-1</sup> h<sup>-1</sup>), showcasing a 3.4 and 1.5 times improvement, respectively. The increased size and anisotropic shape of the multipod Au core contributed to a more potent SPR effect and a more intense localized electric field, resulting in enhanced photocatalytic activity. Integrating multiple enhancement strategies into plasmonic nanostructures, such as light absorption/scattering, plasmon-induced energy transfer, hot electron injection, and plasmonic coupling, can further elevate photocatalytic capabilities. Ren et al. [73] demonstrated this concept by constructing a core-shell satellite (Ag@SiO2@CdS-Au) structured plasmonic photocatalyst, where the Ag NP core efficiently transferred light energy to the CdS shell, and outer Au NPs extended the light response range and generated hot electrons. The resulting plasmonic photocatalyst exhibited a hydrogen evolution rate 200 times higher than a simple CdS photocatalyst, showcasing the synergistic effects of these integrated enhancement strategies. These findings, shown in Figure 9, contribute to the understanding of the structural characteristics and catalytic performance of Au-based nanostructures in various applications, including catalytic reactions and photocatalysis. Figure 9a shows TEM images of Au sphere/ CITS (core-in-tube structure) and Au multipod/CITS core-shell nanostructures. Figure 9b shows the hydrogen evolution of CITS NPs, Au sphere/CITS NPs, and Au multipod/CITS NPs over a 19-h reaction [72]. Figure 9c shows a schematic of the core-shell satellite photocatalyst and the main mechanisms of photocatalytic enhancement. Figure 9d presents the hydrogen evolution rate of the Ag@SiO2@CdS-Au nanostructures with varying Au loading amounts [73].

Among the various semiconductive materials, monoclinic BiVO<sub>4</sub> has gained attention for its application in photoelectrochemical (PEC) catalysis due to three key advantages: (1) a relatively narrow bandgap of 2.4 eV, (2) a suitable valence band position for oxygen evolution, and (3) a favorable conduction band edge position near the thermodynamic hydrogen evolution potential. In a recent study by Chen *et al.* [74], an innovative Au/BiVO<sub>4</sub>/WO<sub>3</sub>/Au nanocomposite photoanode was proposed, employing an antenna/ spacer/reflector architecture for plasmon-enhanced PEC

water splitting. The underlying Au layer collected current and reflected incident light. At the same time, small Au NPs on the surface acted as antennas to trap both incident and reflected light, concentrating solar energy onto the BiVO<sub>4</sub> layer in between. The coupling interaction between the Au layer and Au NPs generated a strong electromagnetic field in the BiVO<sub>4</sub> spacer, promoting efficient charge separation. Wei *et al.* [75] have recently engineered heterostructures comprising AgPt alloy-tipped Au nanostars, revealing remarkable electrocatalytic prowess in the HER

under visible to near-infrared (vis–NIR) light, surpassing performance under dark conditions. This heightened efficiency is ascribed to light-excited hot electrons in Au nanostars and the ensuing electron transfer from Au to AgPt alloy.

Consequently, the AgPt-tipped Au nanostars demonstrated a Tafel slope of 35 mV dec<sup>-1</sup> under vis–NIR light and a low overpotential of 58 mV at a 10 mA cm<sup>-2</sup> current density. While platinum-based materials stand out as superb electrocatalysts for HER, their widespread

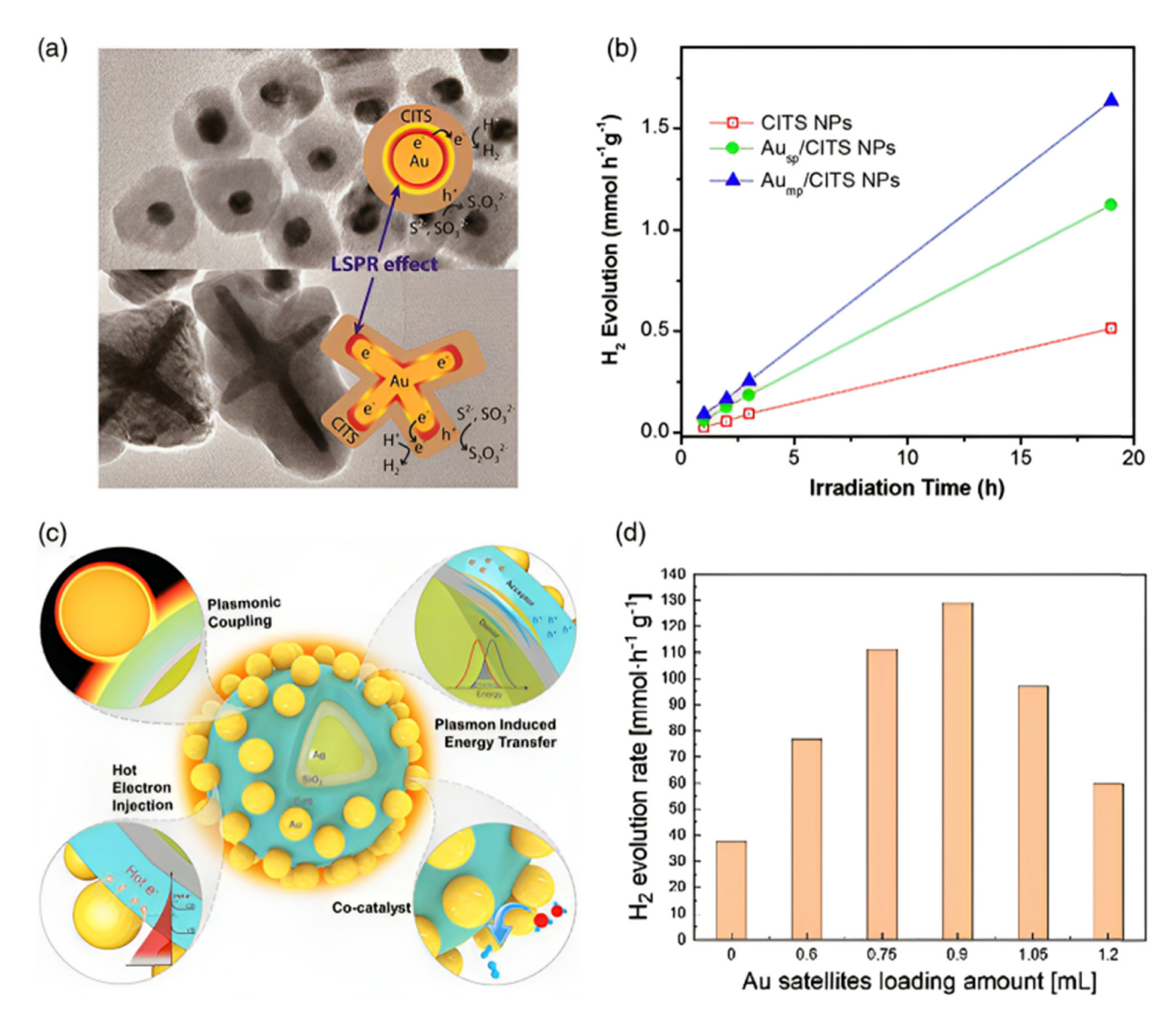


**Figure 9:** Provides valuable insights into the characteristics and performance of different Au-based nanostructures in catalytic and photocatalytic applications. (a) TEM images showcase two core-shell nanostructure types: Au sphere/CITS and Au multipod/CITS. (b) Results of hydrogen evolution experiments for three different samples: CITS NPs, Au sphere/CITS NPs, and Au multipod/CITS NPs. The graph demonstrates the hydrogen evolution rates over a 19-h reaction period, indicating the catalytic performance of each sample. The comparison shows the enhanced catalytic activity of the Aubased core-shell nanostructures compared to the CITS NPs alone. Copyright 2015, American Chemical Society [72]. (c) A core-shell satellite photocatalyst schematic is depicted. (d) provides insights into the effect of Au loading on the hydrogen evolution rate, indicating the optimal Au loading amount for achieving the highest catalytic activity. Copyright 2021, American Chemical Society [73].

application is hindered by excessive costs and scarcity. In this vein, non-noble-metal-based molybdenum disulfide (MoS<sub>2</sub>) emerges as a promising alternative due to its impressive catalytic activity at edge sites, with the unsaturated sulfur atoms along the MoS<sub>2</sub> edge exhibiting a superior affinity for hydrogen [76]. The following studies highlight the potential of utilizing plasmonic effects induced by Au NPs to enhance the catalytic performance of materials for water splitting. By leveraging the light absorption and plasmon-induced effects of Au NPs, researchers can promote catalytic reactions and improve the efficiency of the HER and OER, which are essential steps in overall water-splitting processes.

Du et al. [77] conducted a study on plasmonic electrocatalysts for water splitting by combining GNPs with conventional NiCo-layered double hydroxide (LDH). The researchers aimed to investigate the catalytic sites on the Au/NiCo LDH nanocomposites. They analyzed the overpotential of Au/NiCo LDH after coating the Au NPs with thiophenol. The results showed a significant increase in overpotential for water reduction, indicating that the HER predominantly occurred on the Au surface. Conversely, there was no apparent change in the overpotential for water oxidation, suggesting that the OER primarily occurred on the NiCo LDH surface. The Au/ NiCo LDH catalysts prepared in this study exhibited a low Tafel slope of 57.5 mV dec<sup>-1</sup>, a high hydrogen production rate of 0.369 mmol h<sup>-1</sup>, and an oxygen production rate of 0.184 mmol h<sup>-1</sup> under visible light irradiation. These findings demonstrate the potential of Au/NiCo LDH nanocomposites as efficient electrocatalysts for water splitting, specifically for the HER. In another study by Liu et al. [78], Ni(OH)<sub>2</sub> nanosheets were decorated with Au NPs to enhance the OER performance. The Ni(OH)2-Au hybrid catalysts exhibited improved electrocatalytic OER performance compared to individual Au or Ni(OH)<sub>2</sub> catalysts when illuminated by a 532 nm laser, which is close to the resonance wavelength of Au NPs. The overpotential at a current density of 10 mA cm<sup>-2</sup> was reduced from 330 to 270 mV, and the Tafel slope decreased from 43 to 35 mV dec<sup>-1</sup> under light irradiation. This improvement was attributed to the plasmon-excited hot electrons that promoted the generation of active Ni species and facilitated charge transfer from Ni(OH)<sub>2</sub> nanosheets to Au NPs.

Furthermore, Xu *et al.* [79] designed Au–MnO<sub>2</sub> composite catalysts, where 2D MnO<sub>2</sub> nanosheets acted as primary OER catalysts and Au NPs served as plasmonic exciters. Under 532 nm laser irradiation, effective electron trappers were generated on the Au surface, confining the outer electron of Mn<sup>4+</sup> and forming active Mn<sup>n+</sup> species. These species could extract electrons from OH<sup>-</sup> and facilitate oxygen evolution. The researchers observed an abrupt and significant oxygen evolution and suppression corresponding to the

laser-on and laser-off conditions, as demonstrated by the I-t curve of the Au-MnO<sub>2</sub> composite catalysts.

Catalysis utilizing sunlight as a driving force plays a central role in clean energy conversion, enabling the production of fuels and chemicals by converting abundant natural resources and greenhouse gases. In recent years, significant progress has been made in plasmon-enhanced solar energy conversion through various technologies such as photocatalysis, electro-assisted photocatalysis (PEC), and photo-assisted electrocatalysis. This review summarizes the recent research advancements in these areas. One of the critical factors in plasmon-enhanced solar energy conversion is the LSPR effects of plasmonic metal nanostructures. These nanostructures, including metals like gold (Au), silver (Ag), aluminum (Al), and copper (Cu), have been combined with semiconductors such as TiO2, zinc oxide (ZnO), iron oxide (Fe<sub>2</sub>O<sub>3</sub>), graphitic carbon nitride (g-C3N4), cadmium sulfide (CdS), cadmium selenide (CdSe), and bismuth vanadate (BiVO<sub>4</sub>) to create composite nanostructures. These composite nanostructures utilize the unique properties of each component, resulting in improved catalytic performance. However, despite these advancements, there are challenges for practical applications and largescale production.

One challenge is the limited utilization of sunlight and the lack of high-performance photocatalysts. While photocatalytic systems and PEC cells have been widely studied, they still face limitations in achieving high kinetics of multiple electron/hole transfer processes and working without the presence of electron donors. In this regard, photoassisted electrolysis has emerged as a promising approach to enhance energy conversion efficiency and facilitate water splitting for hydrogen and oxygen production. There is still limited research in plasmon-enhanced photo-assisted electrocatalysis, and several essential issues must be addressed. First, a deeper understanding of the mechanisms of plasmons and electrons in the reaction is necessary to create more rational plasmonic nanostructures that can achieve higher sunlight utilization efficiency and better photocatalytic activity [80]. While plasmonic photocatalysts have mainly been constructed based on the hot electron injection mechanism, other enhancement mechanisms, such as light trapping and plasmon-induced resonance energy transfer (PIRET), should also be considered [81]. Second, the structural design of catalysts plays a vital role in increasing solar energy conversion efficiency [82]. The selection of plasmonic materials with desired optical properties and semiconductors with suitable band gaps is crucial. By utilizing plasmonic materials with resonance within the visible or near-infrared (NIR) range and semiconductors with bandgaps below 2.5 eV, the three dominant plasmonic

energy transfer mechanisms (light trapping, hot electron injection, and PIRET) can be fully utilized, leading to maximized solar energy conversion efficiency and enhanced catalytic activity. Third, integrating different nanomaterials into a stable and compatible system is a challenging task. It requires flexible combinations of available technical conditions, such as seed-mediated growth methods, interface self-assembly engineering, electrostatic interaction-based assembly, and in situ growth [83]. The goal is to obtain ideal and stable catalyst structures while minimizing multistep and time-consuming processes. Finally, advanced techniques are needed to monitor the reaction process and gain insight into the fundamental mechanisms. Experimental methods, particularly in situ surface-enhanced Raman spectroscopy, can provide valuable information on the structural characteristics of reactants and intermediate products with high sensitivity and spatial resolution.

In conclusion, plasmon-enhanced solar energy conversion has shown great potential for clean energy conversion in catalysis. Advances in photocatalytic, PEC, and photoassisted electrocatalytic technologies have paved the way for the efficient utilization of sunlight and producing valuable fuels and chemicals [84]. However, further research is needed to address challenges related to mechanism understanding, structural design, material integration, and advanced monitoring techniques. Plasmon-enhanced catalysis can contribute significantly to developing sustainable energy solutions by tackling these issues.

## 4.2 GNPs in hydrogen storage materials

Despite promising progress, several challenges persist in employing Au NPs to enhance hydrogen storage capacities. First, the enhancement mechanisms are poorly understood and require further theoretical studies [85]. Second, the Au NP synthesis and integration processes need better optimization to maximize dispersion while minimizing costs [86]. Finally, more research is required under practical conditions to validate the real-world viability [87]. Nonetheless, the unique and tunable properties of Au NPs provide endless opportunities to tackle the limitations of various hydrogen storage materials. Standard methods to synthesize Au NPdoped hydrogen storage materials include wet-impregnation, solvothermal/hydrothermal reactions, and atomic layer deposition. Wet impregnation involves simply mixing a solution of Au NPs with the storage material, but aggregation issues lower NP dispersion [88].

On the other hand, solvothermal methods allow in situ growth of well-dispersed Au NPs but involve more complex processing. Atomic layer deposition enables precise control over Au NP size and distribution, although scaling up the process remains challenging. Metal hydrides are promising candidates for solid-state hydrogen storage applications. The most studied example is sodium alanate (NaAlH<sub>4</sub>), which can reversibly store 5.6 wt% of hydrogen but suffers from unfavorable thermodynamics and slow kinetics. Researchers have shown that doping NaAlH4 with Au NPs can lower its hydrogen desorption temperature by over 100°C and improve reaction rates [89]. This is attributed to Au NPs facilitating the dissociation and diffusion of hydrogen on the surface. Other metal hydrides like magnesium hydride and lithium amide have also displayed enhanced hydrogen storage properties with Au NP doping.

Au NPs in MOFs and COFs metal-organic frameworks (MOFs) and covalent organic frameworks (COFs) are porous materials with large surface areas for hydrogen adsorption. However, the binding between hydrogen and the frameworks is often weak, resulting in low storage capacities at room temperature. Studies have shown that impregnating MOFs/COFs with Au NPs introduces stronger binding sites through "spillover" effects. For example, a Zn-based MOF showed a three-fold increase in hydrogen uptake capacity at 1 bar pressure after loading with Au NPs. Additionally, Au NPs can serve as catalytic sites to improve hydrogenation kinetics.

Au NPs in other nanostructures besides the above materials have been incorporated into various carbon-based nanostructures (nanotubes, aerogels, and templates) and polymer scaffolds to enhance hydrogen storage. The high surface-to-volume ratio of the nanostructures increases contacts with Au NPs to maximize spillover effects. Meanwhile, polymers like polyethylene glycol provide a flexible scaffold stabilizing Au NPs while allowing hydrogen mobility. Overall, optimizing the Au NP dispersion is crucial to strike a balance between hydrogen mobility and binding affinity.

# 4.3 Mechanistic insights into catalytic hydrogen storage using nanogold

One of the main mechanisms involved in catalytic hydrogen storage using nanogold is the dissociative adsorption of molecular hydrogen (H2) on the gold surface. GNPs possess a high surface-to-volume ratio, which provides many active sites for hydrogen adsorption. The weak interaction between gold and hydrogen allows for the facile dissociation of H2 molecules into atomic hydrogen (H\*) on the gold surface. This step is considered one of the critical processes in catalytic

hydrogen storage. The dissociated hydrogen atoms (H\*) can then diffuse and migrate on the gold surface, interacting with other hydrogen atoms to form hydrogen clusters or hydride species. The formation of these hydrogen clusters or hydride species on the gold surface contributes to hydrogen storage. The reversible nature of the hydrogen adsorption and desorption process on GNPs allows for the release of hydrogen when needed. The size and morphology of GNPs play a vital role in catalytic hydrogen storage. Smaller NPs typically exhibit higher catalytic activity and hydrogen storage capacity due to their larger surface area and higher density of active sites. Defects, edges, and corners on the NP surface can enhance hydrogen adsorption and facilitate dissociation. Another essential factor influencing catalytic hydrogen storage using nanogold is the presence of support materials. GNPs are often supported on various materials such as metal oxides (e.g., TiO2 and cerium oxide), carbon-based materials (e.g., carbon nanotubes and graphene), and MOFs. The support materials can provide stability to the GNPs, improve the dispersion of NPs, and enhance the overall catalytic performance. The support materials can also interact with GNPs, influencing the electronic properties of gold and modulating the hydrogen adsorption and desorption kinetics. For instance, metal oxide supports can donate or accept electrons, altering the charge distribution on the gold surface and affecting the strength of the hydrogen-gold interaction. This electronic interaction between the support and GNPs can significantly impact the catalytic activity and hydrogen storage properties.

Furthermore, other metal species in alloyed or bimetallic NPs can enhance the catalytic performance for hydrogen storage. For example, the addition of transition metals such as palladium (Pd), platinum (Pt), or nickel (Ni) to GNPs can create alloyed or core-shell structures, which can improve hydrogen adsorption and desorption kinetics [90]. Synergistic effects between different metals can enhance the overall catalytic activity and stability. Anisotropic overgrowth of TiO<sub>2</sub> on gold nanorods (AuNRs) has been demonstrated as a promising structure for achieving plasmon-enhanced hydrogen production through water reduction under visible and NIR light irradiation [91]. This unique structure satisfies the electron refilling requirement and exhibits efficient catalytic activity. The plasmon-enhanced photocatalysis mechanism in this system is attributed to plasmonic hot electron transfer, which occurs due to the LSPR of AuNRs [92]. The LSPR effect is highly dependent on the configuration and architecture of the metal/semiconductor heterojunction, specifically the AuNRs and TiO<sub>2</sub> overgrowth. It is worth noting that the PIRET mechanism, which is based on the inactivity of the core/shell structure, does not play a significant role in this system. The anisotropic overgrowth of TiO2 on AuNRs offers

several advantages for plasmon-enhanced hydrogen production. First, the presence of  ${\rm TiO_2}$  provides a suitable semiconductor material with desirable bandgap properties.  ${\rm TiO_2}$  is well-known for its photocatalytic activity and ability to generate electron-hole pairs upon light absorption. By coupling  ${\rm TiO_2}$  with plasmonic AuNRs, the system benefits from the localized electric field enhancement and hot electron generation resulting from the LSPR effect.

Furthermore, the anisotropic overgrowth ensures the  ${\rm TiO_2}$  layer covers the entire AuNRs surface while maintaining the nanorods' exposed facets. This structure enables efficient charge separation and transfer between the AuNRs and  ${\rm TiO_2}$ , satisfying the electron refilling requirement for sustainable photocatalysis. The exposed aspects of the AuNRs serve as active sites for the catalytic reaction, enhancing the overall hydrogen production efficiency. Under visible and NIR light irradiation, the plasmonic hot electrons generated by the LSPR of the AuNRs are transferred to the  ${\rm TiO_2}$  layer. This transfer of hot electrons is crucial in initiating and driving the water reduction reaction, leading to hydrogen production. The plasmon-enhanced hot electron transfer mechanism is responsible for this system's significant improvement in catalytic activity.

The effectiveness of plasmon-enhanced photocatalysis in this structure is primarily attributed to the localized SPR of the AuNRs. The LSPR effect induces a strong local electromagnetic field enhancement, facilitating the absorption of visible and NIR light by the TiO<sub>2</sub> layer. This enhanced light absorption, combined with the efficient transfer of plasmonic hot electrons to the TiO<sub>2</sub>, improves photocatalytic performance for hydrogen production. It is important to note that the PIRET mechanism, which relies on coreshell structures, does not contribute significantly to the observed catalytic activity in this system. The absence of a significant role for PIRET further emphasizes the importance of the plasmonic hot electron transfer mechanism in this anisotropic overgrowth structure.

In summary, the anisotropic overgrowth of TiO<sub>2</sub> on AuNRs provides a unique structure that satisfies the electron refilling requirement and exhibits efficient plasmonenhanced hydrogen production through water reduction [93]. The plasmon-enhanced photocatalysis mechanism in this system is primarily attributed to the plasmonic hot electron transfer mechanism, which occurs due to the localized SPR of AuNRs. This structure holds great promise for developing efficient and sustainable photocatalytic systems for clean energy conversion. Wu *et al.* [93] developed a wet-chemistry method to synthesize anisotropic AuNR/TiO<sub>2</sub> NDs for plasmon-enhanced photocatalysis through selective TiO<sub>2</sub> deposition on AuNR tips. The researchers found that cetyltrimethylammonium bromide (CTAB)

surfactant assembles differently on the tips and sides of AuNRs. CTAB forms a less dense bilayer on the tips due to their curvature. This allows titanium species to access the tips and selectively deposit TiO2, forming the anisotropic ND structure. The concentration, alkyl chain length, and diameter of the AuNRs influence the selective TiO2 deposition. An appropriate CTAB concentration between its first and second critical micelle concentrations gives the highest yield of tipped TiO<sub>2</sub> coating. Shorter chain CTABs like C12TAB enable tip-selective coating of thinner AuNRs. The resulting AuNR/TiO<sub>2</sub> NDs exhibit plasmonenhanced hydrogen evolution and methylene blue (MB) photoreduction under visible light. This is attributed to the spatial separation of the Au and TiO2 regions, which allows hot electrons from the AuNRs to access the TiO2 for reduction reactions. In contrast, oxidation reactions occur on the exposed AuNR sides.

In contrast, AuNR@TiO<sub>2</sub> core—shell NPs show little photocatalytic activity. The anisotropic overgrowth of TiO<sub>2</sub> on AuNRs is demonstrated through detailed characterization using TEM and high-angle annular dark-field scanning

transmission electron microscopy with energy-dispersive EDX (HAADF-STEM-EDX) analyses (Figure 10). The resulting structure reveals two symmetrical caps made from porous  $TiO_2$  with fundamental building blocks <2 nm in size. The deposition process exhibits specific tip-side selectivity, as confirmed by the absence of Ti signal in transverse scanning through the lateral side. Linear scanning in the longitude direction highlights a transparent signal distribution, emphasizing the controlled and uniform growth of the two  $TiO_2$  caps. The observed distribution difference and cap shapes suggest that the anisotropic  $TiO_2$  deposition initiates from two tips of each AuNR and extends toward the middle side surface, providing insights into this nanomaterial's well-defined and organized growth mechanism.

The notable feature of the designed AuNR/TiO<sub>2</sub> NDs lies in their remarkable capability to induce SPR-enhanced hotelectron generation under visible and NIR light (Figure 11). In contrast to AuNR@TiO<sub>2</sub> core—shell NPs and pure amorphous TiO<sub>2</sub>, which exhibit no activity for hydrogen (H<sub>2</sub>) evolution, AuNR/TiO<sub>2</sub> NDs demonstrate significantly elevated photoactivity, surpassing physically mixed AuNRs

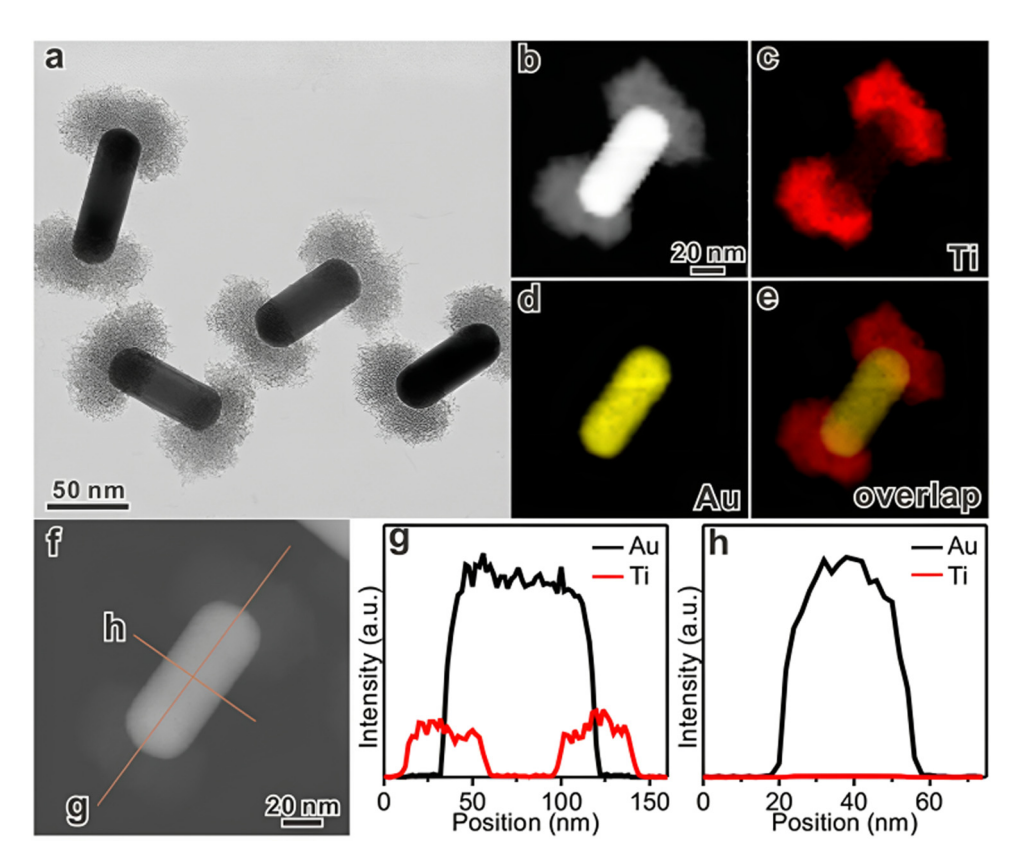


**Figure 10:** Comprehensive characterization of AuNR/TiO<sub>2</sub> NDs, with (a) showcasing a TEM image. (b)–(e) High-angle annular dark-field scanning transmission electron microscopy (HAADF-STEM) views along with elemental maps, offering insights into the distribution of gold (Au) and titanium (Ti) within the nanorods. (f)–(h) Elemental profiles, providing quantitative data on the composition along specific regions of the AuNR/TiO<sub>2</sub> NDs. This multi-modal analysis allows for a detailed examination of the structural and elemental characteristics, enhancing our understanding of the nanostructure's composition and morphology. Copyright and permission from the study of Wu *et al.* [93].

and amorphous TiO<sub>2</sub>. The observed difference in photoactivity cannot be attributed to surface area or the mass of TiO<sub>2</sub>, as amorphous TiO<sub>2</sub> itself does not absorb visible light, and an excess quantity of TiO<sub>2</sub> was used in the mechanical mixture. The unique ND structure, characterized by intimate physical contact and strong plasmonic coupling, is pivotal in enhancing charge separation for plasmon-enhanced photocatalysis. Control experiments further underline the importance of the ND structure, and the higher activity of AuNR/TiO<sub>2</sub> NDs compared to the spherical GNPs on crystalline TiO<sub>2</sub> suggests the significance of the nanodisk (ND) architecture. The plasmon-enhanced photocatalysis mechanism is proposed to involve plasmonic hot electron transfer due to localized SPR of AuNRs, dependent on the metal/semiconductor

heterojunction's configuration and architecture, rather than PIRET, as indicated by the inactivity of the core—shell structure. This mechanism is further demonstrated through the photoreduction of MB, emphasizing the versatility and potential applications of AuNR/TiO<sub>2</sub> NDs in various catalytic processes. Figure 11 presents a comprehensive comparison of catalytic activities and photoreduction processes under visible illumination for multiple catalysts. Figure 11(a) depicts the hydrogen (H<sub>2</sub>) evolution rate by different catalysts, highlighting the significantly enhanced activity of AuNR/TiO<sub>2</sub> NDs compared to other configurations, such as AuNR@TiO<sub>2</sub> core/shell NPs and physically mixed AuNRs with amorphous TiO<sub>2</sub>. Figure 11(b) shows the normalized concentration of MB over irradiation time in the presence

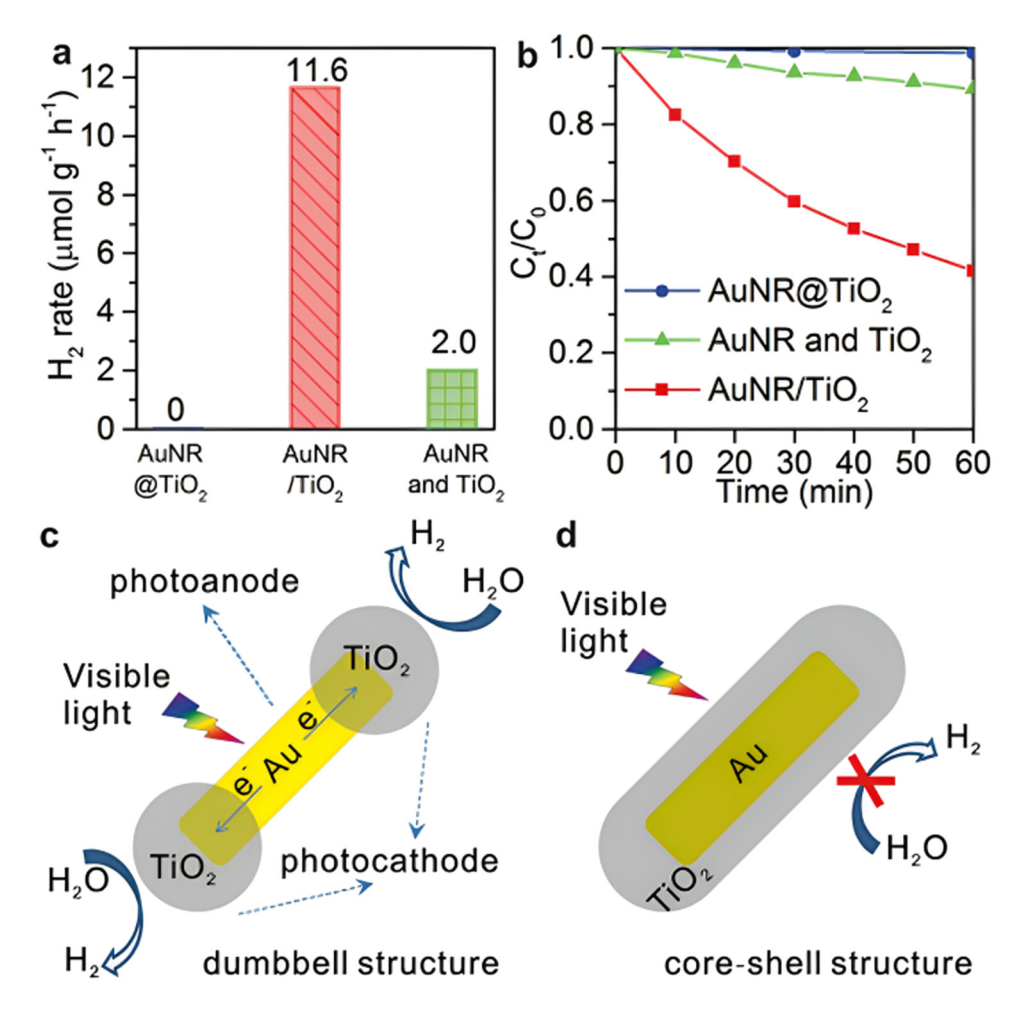


**Figure 11:** Comparative analysis of catalytic activities and photoreduction processes under visible illumination. (a) Hydrogen (H<sub>2</sub>) evolution rate by various catalysts. AuNR/TiO<sub>2</sub> NDs exhibit significantly enhanced activity compared to other configurations, such as AuNR@TiO<sub>2</sub> core/shell NPs and physically mixed AuNRs with amorphous TiO<sub>2</sub>. (b) Normalized MB concentration over irradiation time in the presence of methanol and water. AuNR/TiO<sub>2</sub> NDs demonstrate effective photoreduction reactions, as shown by the decreasing concentration of MB. (c) Structural and operational mechanism under visible light for an individual AuNR/TiO<sub>2</sub> dumbbell. Plasmonic AuNRs generate hot electrons filtered by the Au/TiO<sub>2</sub> Schottky barrier, enabling efficient photoreduction and highlighting the distinctive operation mechanism for the AuNR/TiO<sub>2</sub> NDs. (d) Structural and operational mechanism under visible light for a core–shell AuNR@TiO<sub>2</sub> structure. Plasmonic hot electrons are not efficiently transferred and utilized for photoreduction, resulting in lower activity. Copyright and permission from the study of Wu *et al.* [93].

of methanol and water, demonstrating the effectiveness of AuNR/TiO<sub>2</sub> NDs in photoreduction reactions. The structural and operational mechanisms under visible light are illustrated in Figure 11(c) and (d), detailing an individual AuNR/TiO2 dumbbell and a core/shell AuNR@TiO2 structure. In Figure 11(c), plasmonic AuNRs generate hot electrons filtered by the Au/TiO2 Schottky barrier for efficient photoreduction, highlighting the distinctive operation mechanism for the AuNR/TiO<sub>2</sub> NDs. A bottom-up, wet-chemistry technique has been developed for synthesizing anisotropic TiO<sub>2</sub> overgrowth on AuNRs. This method involves the selective spatial assembly of a CnTAB bilayer on the surfaces of AuNRs and the hydrolysis of TiCl<sub>3</sub>. The concentration, alkyl chain length of CnTAB, and diameter of AuNRs are crucial in controlling the selective overgrowth process.

The resulting AuNR/TiO<sub>2</sub> NDs exhibit plasmon-enhanced hydrogen (H<sub>2</sub>) evolution under visible/NIR light. The interface between AuNRs and TiO<sub>2</sub>, with the AuNR side exposed, forms a Schottky junction that can filter out SPR hot electrons from the AuNRs. This unique structure enables efficient plasmoninduced H2 evolution. Furthermore, the activity of the AuNR/ TiO<sub>2</sub> NDs for plasmon-induced H2 evolution can be further improved by engineering the structure, such as by loading cocatalysts. This additional modification has the potential to enhance the overall catalytic activity.

# 5 Toward real-world applications in hydrogen storage technologies

AuNCs have been explored for environmental applications for degrading organic pollutants via enhanced catalysis, detecting heavy metal ions and pesticides through fluorescence quenching, and enabling solar-driven water purification. Mechanisms and processes and several features of AuNCs underpin their versatile applicability in energy storage and environmental treatment - high specific surface area (up to 50 m<sup>2</sup>/g), quantum confinement effects, plasmonic resonance, appropriate band positions, and excellent electrocatalytic activity. In Li-based batteries, ultra-small AuNCs boost charge transfer kinetics and limit polysulfide shuttling in Li-S cells, enhancing coulombic efficiency to over 90%. Doping Zn-air cathode with AuNCs lowers overpotential by more than 50 mV while suppressing CO<sub>2</sub> conversion [94]. All these effects rely on electrocatalysis facilitated by high surface area exposure of Au atoms with unfilled 6s orbitals, resonating with intermediates, and accelerating redox reactions. AuNCs improve specific capacitance for supercapacitor electrodes by over 76% when incorporated into MnO2 via combined EDLC and

pseudocapacitive charge storage. Other reports have shown specific capacitance enhancement by 91% for rGO electrodes with AuNC additives [95].

In both cases, metallic AuNCs facilitate fast ion diffusion and redox reactions. In photocatalytic environmental remediation, AuNCs exhibit plasmon resonance, enabling visible light harvest and hot carrier generation - leading to improved degradation rates of Rhodamine B (4-fold), microcystin-LR (7.5-fold), and other persistent organic pollutants under solar irradiation. Similar hot carrier effects also facilitate AuNC-mediated photodecomposition of phenol and oxidative desulfurization. For fluorescent detection of hazardous heavy metal ions (like Hg<sup>2+</sup>, Ag<sup>+</sup>, and Cu<sup>2+</sup>) [96], AuNCs provide selective quenching platforms based on interactions with specific functional groups on the metal ion surface. Sensitivities up to part-per-trillion levels have been achieved for batch-based measurements of contaminated water samples. Safety considerations despite promising applications, the long-term safety, environmental persistence, and bioaccumulation risks of AuNCs need to be evaluated more systematically. Since the toxicity of NPs is strongly dependent on multiple parameters like shape, surface chemistry, dose, and exposure route, developing categorical regulations is difficult.

Nevertheless, responsible life cycle analysis covering the production, use, recycling, and disposal of AuNCs must be standardized through collaborations between researchers, industries, and regulatory agencies. Additional environmental toxicology studies are required to supplement existing preliminary cytotoxicity data. Ethical guidelines regarding AuNC applications in biomedicine, agriculture, and food technology can be implemented to promote transparency, accountability, and public welfare. AuNCs have emerged as attractive materials for diverse applications due to their unique optoelectronic properties derived from the ultra-small size regime. Energy storage and environmental remediation are two key domains where AuNCs have already shown tangible enhancements and promise further development. However, large-scale adoption and commercial viability require systematic safety and life cycle analyses to supplement the excitement around proof-ofconcept studies. Overall, AuNCs represent a critical addition to the nanomaterial toolkit, with opportunities for sustained research and responsible innovation.

### 6 Conclusions

This comprehensive review delves into recent advancements in leveraging GNPs to enhance diverse materials' hydrogen storage capacities and kinetics. The distinctive physicochemical properties of Au NPs are pivotal in driving these enhancements. Nanoscale Au NPs establish optimal contact with storage materials with a high surface-tovolume ratio, maximizing spillover effects for efficient hydrogen absorption. The catalytic activity of Au NPs facilitates hydrogen dissociation and diffusion, while their tunable electronic structure allows for tailored hydrogen adsorption strengths. Defect sites created by Au NPs synergistically complement their dissociation ability. Numerous studies show significant improvements in the hydrogen storage capacities of materials such as metal hydrides, MOFs, and nanostructured carbons upon integrating with Au NPs. These advancements, addressing fundamental limitations like poor thermodynamic stability and slow kinetics, promise practical viability for hydrogen storage candidates. The review further explores synthesis strategies for incorporating Au NPs, emphasizing the need to optimize dispersion and interfacial contacts. Prospects highlight the necessity for in-depth mechanistic studies, scalable fabrication strategies, validation under practical conditions, incorporation into devices, and techno-economic analyses to propel the deployment of Au NP-enhanced hydrogen materials in real-world applications. In essence, harnessing the unique properties of Au NPs presents a promising and eco-friendly strategy to overcome hydrogen storage limitations, marking a significant step toward realizing the hydrogen economy. Achieving this vision requires interdisciplinary efforts in fundamental sciences, engineering optimization, and policy support.

**Acknowledgments:** The authors extend their appreciation to the Deanship of Scientific Research at Northern Border University, Arar, KSA, for funding this research work through the project number "NBU-FFR-2024-2618-04".

**Funding information:** The authors extend their appreciation to the Deanship of Scientific Research at Northern Border University, Arar, KSA, for funding this research work through the project number "NBU-FFR-2024-2618-04".

**Author contributions:** All authors have accepted responsibility for the entire content of this manuscript and approved its submission.

**Conflict of interest:** The authors state no conflict of interest.

### References

[1] Khan IM, Niazi S, Akhtar W, Yue L, Pasha I, Khan MKI, et al. Surface functionalized AuNCs optical biosensor as an emerging food safety

- indicator: Fundamental mechanism to future prospects. Coord Chem Rev. 2023:474:214842.
- [2] Goncalves JM, Kumar A, da Silva MI, Toma HE, Martins PR, Araki K, et al. Nanoporous gold-based materials for electrochemical energy storage and conversion. Energy Technol. 2021;9(5):2000927.
- [3] Sikiru S, Oladosu TL, Amosa TI, Olutoki JO, Ansari MNM, Abioye KJ, et al. Hydrogen-powered horizons: Transformative technologies in clean energy generation, distribution, and storage for sustainable innovation. Int J Hydrog Energy. 2024;56:1152–82.
- [4] Wittstock G, Bäumer M, Dononelli W, Klüner T, Lührs L, Mahr C, et al. Nanoporous gold: From structure evolution to functional properties in catalysis and electrochemistry. Chem Rev. 2023;123(10):6716–92.
- [5] Ishida T, Murayama T, Taketoshi A, Haruta M. Importance of size and contact structure of gold nanoparticles for the genesis of unique catalytic processes. Chem Rev. 2019;120(2):464–525.
- [6] Guo C, Xu M, Tao Z, Liu J, Zhang S, He L, et al. Understanding electron structure of covalent triazine framework embraced with gold nanoparticles for nitrogen reduction to ammonia. J Colloid Interface Sci. 2024;675:369–78.
- [7] Ghobashy MM, Alkhursani SA, Alqahtani HA, El-damhougy TK, Madani M. Gold nanoparticles in microelectronics advancements and biomedical applications. Mater Sci Eng: B. 2024;301:117191.
- [8] Ielo I, Rando G, Giacobello F, Sfameni S, Castellano A, Galletta M, et al. Synthesis, chemical–physical characterization, and biomedical applications of functional gold nanoparticles: A review. Molecules. 2021;26(19):5823.
- [9] Wang C, Astruc D. Recent developments of nanocatalyzed liquid-phase hydrogen generation. Chem Soc Rev. 2021;50(5):3437–84.
- [10] Tahir MB, Rafique MS, Sagir M, Malik MF. New insights in photocatalysis for environmental applications. Singapore: Springer; 2022.
- [11] Behera P, De M. Surface-engineered nanomaterials for optical array based sensing. ChemPlusChem. 2024;89(5):e202300610.
- [12] Rezaei B, Yari P, Sanders SM, Wang H, Chugh VK, Liang S, et al. Magnetic nanoparticles: a review on synthesis, characterization, functionalization, and biomedical applications. Small. 2024;20(5):2304848.
- [13] Shabaka S, Moawad MN, Ibrahim MIA, El-Sayed AAM, Ghobashy MM, Hamouda AZ, et al. Youssef, prevalence and risk assessment of microplastics in the Nile Delta estuaries: "The Plastic Nile" revisited. Sci Total Environ. 2022;852:158446.
- [14] Ghani SAA, El-Sayed AAM, Ibrahim MIA, Ghobashy MM, Shreadah MA, Shabaka S. Characterization and distribution of plastic particles along Alexandria beaches, Mediterranean Coast of Egypt, using microscopy and thermal analysis techniques. Sci Total Environ. 2022;834:155363.
- [15] El-Sayed AAM, Ibrahim MIA, Shabaka S, Ghobashy MM, Shreadah MA, Ghani SAA. Microplastics contamination in commercial fish from Alexandria City, the Mediterranean Coast of Egypt. Environ Pollut. 2022;313:120044.
- [16] Ghobashy MM, Elbarbary AM, Hegazy DE, Maziad NA. Radiation synthesis of pH-sensitive 2-(dimethylamino) ethyl methacrylate/ polyethylene oxide/ZnS nanocomposite hydrogel membrane for wound dressing application. J Drug Deliv Sci Technol. 2022;73:103399.
- [17] Abd El-Sattar NEA, El-Hddad SESA, Ghobashy MM, Zaher AA, El-Adl K. Nanogel-mediated drug delivery system for anticancer agent: pH stimuli responsive poly (ethylene glycol/acrylic acid)

nanogel prepared by gamma irradiation. Bioorg Chem. 2022:127:105972.

**DE GRUYTER** 

- [18] Alkhursani SA, Ghobashy MM, Al-Gahtany SA, Meganid AS, Abd El-Halim SM, Ahmad Z, et al. Application of nano-inspired scaffoldsbased biopolymer hydrogel for bone and periodontal tissue regeneration. Polymers. 2022;14(18):3791.
- [19] Ghobashy MM, Mousaa IM, El-Sayyad GS. Radiation synthesis of urea/hydrogel core shells coated with three different natural oils via a layer-by-layer approach: An investigation of their slow release and effects on plant growth-promoting rhizobacteria. Prog Org Coat. 2021;151:106022.
- [20] Sharma N, Mohammad W, Le Guével X, Shanavas A. Gold nanoclusters as high resolution NIR-II theranostic agents. Chem Biomed Imaging. 2024;2:462-80.
- [21] Wu M, Dong F, Yang Y, Cui X, Liu X, Zhu Y, et al. Emerging atomically precise metal nanoclusters and ultrasmall nanoparticles for efficient electrochemical energy catalysis: Synthesis strategies and surface/interface engineering. Electrochem Energy Rev. 2024:7(1):10.
- [22] Chakraborty S, Babanova S, Rocha RC, Desireddy A, Artyushkova K, Boncella AE, et al. A hybrid DNA-templated gold nanocluster for enhanced enzymatic reduction of oxygen. J Am Chem Soc. 2015;137(36):11678-87.
- [23] Clark JH, Macquarrie DJ. Environmentally friendly catalytic methods. Chem Soc Rev. 1996;25(5):303-10.
- [24] Fereja SL, Chen W. Metal nanoclusters for energy storage applications. Luminescent metal nanoclusters. Sawston, United Kingdom: Elsevier; 2022. p. 625-58.
- [25] Lu P, Xue D, Yang H, Liu Y. Supercapacitor and nanoscale research towards electrochemical energy storage. Int J Smart Nano Mater. 2013;4(1):2-26.
- [26] Khosropour H, Keramat M, Tasca F, Laiwattanapaisal W. A comprehensive review of the application of Zr-based metal-organic frameworks for electrochemical sensors and biosensors. Microchim Acta. 2024;191(8):449.
- [27] Sundararaman S, Chacko J, Prabu D, Karthikeyan M, Kumar JA, Saravanan A, et al. Noteworthy synthesis strategies and applications of metal-organic frameworks for the removal of emerging water pollutants from aqueous environment. Chemosphere. 2024:362:142729.
- [28] Chen W, Liang J, Luo J, Huang Z, Liu F, Li S. On-off-on switchable fluorescent chemosensor based on glutathione-protected gold nanoclusters for high-selective on-site Cr (VI) detection in complex biological samples. Microchem J. 2024;199:110072.
- [29] Wang K, Meng X, Yan X, Fan K. Nanozyme-based point-of-care testing: Revolutionizing environmental pollutant detection with high efficiency and low cost. Nano Today. 2024;54:102145.
- [30] Zhang L, Bi X, Wang H, Li L, You T. Loading of AuNCs with AIE effect onto cerium-based MOFs to boost fluorescence for sensitive detection of Hg<sup>2+</sup>. Talanta. 2024;273:125843.
- [31] Godja N-C, Munteanu F-D. Hybrid nanomaterials: a brief overview of versatile solutions for sensor technology in healthcare and environmental applications. Biosensors. 2024;14(2):67.
- [32] Tomasulo A, Ramakrishna MV. Quantum confinement effects in semiconductor clusters. II, The. J Chem Phys. 1996;105(9):3612-26.
- [33] Cui M, Zhao Y, Song Q. Synthesis, optical properties and applications of ultra-small luminescent gold nanoclusters. TrAC Trends Anal Chem. 2014;57:73-82.

- [34] An K, Somorjai GA. Size and shape control of metal nanoparticles for reaction selectivity in catalysis. ChemCatChem. 2012;4(10):1512-24.
- [35] Casteleiro B, Martinho JMG, Farinha JPS. Encapsulation of gold nanoclusters: stabilization and more. Nanoscale. 2021;13(41):17199-217.
- Bandodkar AJ, Jeerapan I, Wang J. Wearable chemical sensors: present challenges and future prospects. Acs Sens. 2016;1(5):464-82.
- [37] Chahande AM, Maibam A, Krishnamurty S, Devi RN. Ultra-small Au nanoclusters with tailored photoluminescence properties using modified thiol ligands: a computational and experimental demonstration. Part Part Syst Charact. 2024;1:2400011.
- [38] Bhunia S, Mukherjee M, Purkayastha P. Fluorescent metal nanoclusters: prospects for photoinduced electron transfer and energy harvesting. Chem Commun. 2024;60(25):3370-8.
- [39] Behera P, De M. Nanomaterials in optical array-based sensing. Org Inorg Mater Sens. 2024;2:495-533.
- Diriwari PI. Resonance energy transfer within and to optical nanoparticles for bioimaging and biosensing applications. Basel, Switzerland: MDPI; 2024.
- [41] El-Sattar NEAA, El-Hddad SESA, Ghobashy MM, Zaher AA, El-Adl K. Nanogel-mediated drug delivery system for anticancer agent: pH stimuli responsive poly(ethylene glycol/acrylic acid) nanogel prepared by gamma irradiation. Bioorg Chem. 2022;127:105972-87.
- Chen H, Zou L, Hossain E, Li Y, Liu S, Pu Y, et al. Assembly of Au nanoclusters based functional structures and practical applications. Biomater Sci. 2024;12:4283-300.
- Mohseni N, Moodi M, Kefayat A, Shokati F, Molaabasi F. Challenges [43] and opportunities of using fluorescent metal nanocluster-based colorimetric assays in medicine. ACS Omega. 2024;9(3):3143-63.
- [44] Jin R, Higaki T. Open questions on the transition between nanoscale and bulk properties of metals. Commun Chem. 2021;4(1):28.
- [45] Ma J, Yang M, Zhang B, Niu M. The roles of templates consisting of amino acids in the synthesis and application of gold nanoclusters. Nanoscale. 2024;16(15):7287-306.
- [46] Huang H, Zheng Y, Chang M, Song J, Xia L, Wu C, et al. Ultrasoundbased micro-/nanosystems for biomedical applications. Chem Rev. 2024;124:8307-472.
- [47] Hang Y, Wang A, Wu N. Plasmonic silver and gold nanoparticles: shape-and structure-modulated plasmonic functionality for pointof-caring sensing, bio-imaging and medical therapy. Chem Soc Rev. 2024:53:2932-71.
- [48] Pan M, Wang Y, Liu Y, Zhang M, Liu X, Yuan Y, et al. Optimizing interfacial modification for enhanced performance of Na3V2 (PO4) 3 cathode in sodium-ion batteries. Chem Eng J. 2024;495:153396.
- [49] Young SL, Kellon JE, Hutchison JE. Small gold nanoparticles interfaced to electrodes through molecular linkers: a platform to enhance electron transfer and increase electrochemically active surface area. J Am Chem Soc. 2016;138(42):13975-84.
- Im J, Trindade GF, Quach TT, Sohaib A, Wang F, Austin J, et al. Functionalized gold nanoparticles with a cohesion enhancer for robust flexible electrodes. ACS Appl Nano Mater. 2022;5(5):6708-16.
- [51] Bahadur R, Singh G, Li Z, Singh B, Srivastava R, Sakamoto Y, et al. Hybrid nanoarchitectonics of ordered mesoporous C60-BCN with high surface area for supercapacitors and lithium-ion batteries. Carbon. 2024;216:118568.

- [52] Liang Z, Yao Y, Wang H. Recent advancements in polyoxometalate-functionalized fiber materials: A review. Nanotechnol Rev. 2024;13(1):20230199.
- [53] Kar P, Guerra EI, Liao WS. Nanofabrication and sensing technology: from the interface-mediated mechanism point-of-view. Adv Sens Res. 2024;1:2400031.
- [54] Shen M-C, Lai J-C, Hong C-Y, Wang G-J. Electrochemical aptasensor for detecting Der p2 allergen using polycarbonate-based doublegeneration gold nanoparticle chip. Sens Bio-Sens Res. 2017;13:75–80.
- [55] Fadeev M, Kozlovskiy A, Korolkov I, Egizbek K, Nazarova A, Chudoba D, et al. Iron oxide@ gold nanoparticles: Synthesis, properties and potential use as anode materials for lithiumion batteries. Colloids Surf A: Physicochem Eng Asp. 2020;603:125178.
- [56] Chen H, Wang C, Dong W, Lu W, Du Z, Chen L. Monodispersed sulfur nanoparticles for lithium–sulfur batteries with theoretical performance. Nano Lett. 2015;15(1):798–802.
- [57] Ren W, Ma W, Zhang S, Tang B. Recent advances in shuttle effect inhibition for lithium sulfur batteries. Energy Storage Mater. 2019;23:707–32.
- [58] Ye Y, Wu F, Xu S, Qu W, Li L, Chen R. Designing realizable and scalable techniques for practical lithium sulfur batteries: a perspective. J Phys Chem Lett. 2018;9(6):1398–414.
- [59] Sun K, Fu Y, Sekine T, Mabuchi H, Hossain S, Zhang Q, et al. Metal nanoclusters as a superior polysulfides immobilizer toward highly stable lithium–sulfur batteries. Small. 2023;20:2304210.
- [60] Du Y, Sheng H, Astruc D, Zhu M. Atomically precise noble metal nanoclusters as efficient catalysts: a bridge between structure and properties. Chem Rev. 2019;120(2):526–622.
- [61] Marangon V, Di Lecce D, Brett DJL, Shearing PR, Hassoun J. Characteristics of a gold-doped electrode for application in high-performance lithium-sulfur battery. J Energy Chem. 2022:64:116–28
- [62] Zhu W, Yuan H, Liao F, Shen Y, Shi H, Shi Y, et al. Strain engineering for Janus palladium-gold bimetallic nanoparticles: enhanced electrocatalytic performance for oxygen reduction reaction and zinc-air battery. Chem Eng J. 2020;389:124240.
- [63] Nguyen DC, Doan TLL, Prabhakaran S, Kim DH, Kim NH, Lee JH. Rational construction of Au@ Co2N0. 67 nanodots-interspersed 3D interconnected N-graphene hollow sphere network for efficient water splitting and Zn-air battery. Nano Energy. 2021;89:106420.
- [64] Li J, Lou Z, Li B. Engineering plasmonic semiconductors for enhanced photocatalysis. J Mater Chem A. 2021;9(35):18818–35.
- [65] Oshikiri T, Jo H, Shi X, Misawa H. Boosting hydrogen evolution at visible light wavelengths by using a photocathode with modal strong coupling between plasmons and a fabry-pérot nanocavity. Chem – Eur J. 2022;28(24):e202200288.
- [66] Sagadevan S, Podder J, Mohammad F. Metal oxides for optoelectronics and optics-based medical applications. Amsterdam, Netherlands: Elsevier; 2022.
- [67] Bicakova O, Straka P. Production of hydrogen from renewable resources and its effectiveness. Int J Hydrog Energy. 2012;37(16):11563–78.
- [68] Sousa-Castillo A, Comesaña-Hermo M, Rodríguez-González B, Pérez-Lorenzo M, Wang Z, Kong X-T, et al. Boosting hot electrondriven photocatalysis through anisotropic plasmonic nanoparticles with hot spots in Au–TiO2 nanoarchitectures. J Phys Chem C. 2016;120(21):11690–9.

- [69] Nguyen NT, Altomare M, Yoo J, Schmuki P. Efficient photocatalytic H2 evolution: controlled dewetting-dealloying to fabricate siteselective high-activity nanoporous Au particles on highly ordered TiO2 nanotube arrays. Adv Mater. 2015;27(20):3208–15.
- [70] Zhang Z, Zhang L, Hedhili MN, Zhang H, Wang P. Plasmonic gold nanocrystals coupled with photonic crystal seamlessly on TiO2 nanotube photoelectrodes for efficient visible light photoelectrochemical water splitting. Nano Lett. 2013;13(1):14–20.
- [71] Mubeen S, Lee J, Liu D, Stucky GD, Moskovits M. Panchromatic photoproduction of H2 with surface plasmons. Nano Lett. 2015;15(3):2132–6.
- [72] Ha E, Lee LYS, Man H-W, Tsang SCE, Wong K-Y. Morphology-controlled synthesis of Au/Cu2FeSnS4 core–shell nanostructures for plasmon-enhanced photocatalytic hydrogen generation. ACS Appl Mater Interfaces. 2015;7(17):9072–7.
- [73] Ren H, Yang J-L, Yang W-M, Zhong H-L, Lin J-S, Radjenovic PM, et al. Core-shell-satellite plasmonic photocatalyst for broad-spectrum photocatalytic water splitting. ACS Mater Lett. 2020;3(1):69–76.
- [74] Chen B, Zhang Z, Baek M, Kim S, Kim W, Yong K. An antenna/ spacer/reflector based Au/BiVO4/WO3/Au nanopatterned photoanode for plasmon-enhanced photoelectrochemical water splitting. Appl Catal B: Environ. 2018;237:763–71.
- [75] Wei Y, Zhang X, Liu Z, Chen H-S, Yang P. Site-selective modification of AgPt on multibranched Au nanostars for plasmon-enhanced hydrogen evolution and methanol oxidation reaction in visible to near-infrared region. J Power Sources. 2019;425:17–26.
- [76] Cui J, Jiang R, Lu W, Xu S, Wang L. , Plasmon-enhanced photoe-lectrical hydrogen evolution on monolayer  $MoS_2$  decorated Cu1. 75S-Au nanocrystals. Small. 2017;13(8):1602235.
- [77] Du L, Shi G, Zhao Y, Chen X, Sun H, Liu F, et al. Plasmon-promoted electrocatalytic water splitting on metal–semiconductor nanocomposites: the interfacial charge transfer and the real catalytic sites. Chem Sci. 2019;10(41):9605–12.
- [78] Liu G, Li P, Zhao G, Wang X, Kong J, Liu H, et al. Promoting active species generation by plasmon-induced hot-electron excitation for efficient electrocatalytic oxygen evolution. J Am Chem Soc. 2016;138(29):9128–36.
- [79] Xu J, Gu P, Birch DJS, Chen Y. Plasmon-promoted electrochemical oxygen evolution catalysis from gold decorated MnO2 nanosheets under green light. Adv Funct Mater. 2018;28(31):1801573.
- [80] Wang T, Wang H-J, Lin J-S, Yang J-L, Zhang F-L, Lin X-M, et al. Plasmonic photocatalysis: mechanism, applications and perspectives. Chin J Struct Chem. 2023;42(9):100066.
- [81] Abdel Maksoud MI, Ghobashy MM, Kodous AS, Fahim RA, Osman AI, Al-Muhtaseb AA, et al. Insights on magnetic spinel ferrites for targeted drug delivery and hyperthermia applications. Nanotechnol Rev. 2022;11(1):372–413.
- [82] Yang B, Li C, Wang Z, Dai Q. Thermoplasmonics in solar energy conversion: materials, nanostructured designs, and applications. Adv Mater. 2022;34(26):2107351.
- [83] Yang J, Liu H. Metal-based composite nanomaterials. Berlin, Germany: Springer; 2015.
- [84] Changotra R, Ray AK, He Q. Establishing a water-to-energy platform via dual-functional photocatalytic and photoelectrocatalytic systems: A comparative and perspective review. Adv Colloid Interface Sci. 2022;309:102793.
- [85] Schatz GC. Theoretical studies of surface enhanced raman scattering. Acc Chem Res. 1984;17(10):370–6.
- [86] Darabdhara G, Das MR, Singh SP, Rengan AK, Szunerits S, Boukherroub R. Ag and Au nanoparticles/reduced graphene oxide

- composite materials: synthesis and application in diagnostics and therapeutics. Adv Colloid Interface Sci. 2019;271:101991.
- [87] Berger ML, Sox H, Willke RJ, Brixner DL, Eichler HG, Goettsch W, et al. Good practices for real-world data studies of treatment and/or comparative effectiveness: recommendations from the joint ISPOR-ISPE Special Task Force on real-world evidence in health care decision making. Value Health. 2017;20(8):1003–8.
- [88] Kumar A, Choudhary P, Chhabra T, Kaur H, Kumar A, Qamar M, et al. Frontier nanoarchitectonics of graphitic carbon nitride based plasmonic photocatalysts and photoelectrocatalysts for energy, environment and organic reactions. Mater Chem Front. 2023;7(7):1197–247.
- [89] Lesch DA, Adriaan Sachtler JWJ, Low JJ, Jensen CM, Ozolins V, Siegel D, et al. Discovery of novel complex metal hydrides for hydrogen storage through molecular modeling and combinatorial methods. Des Plaines, Illinois, United States: UOP LLC, A Honeywell Company; 2011.
- [90] Bhalothia D, Krishnia L, Yang S-S, Yan C, Hsiung W-H, Wang K-W, et al. Recent advancements and future prospects of noble metal-based heterogeneous nanocatalysts for oxygen reduction and hydrogen evolution reactions. Appl Sci. 2020;10(21):7708.

- [91] Costi R, Saunders AE, Banin U. Colloidal hybrid nanostructures: a new type of functional materials. Angew Chem Int Ed. 2010;49(29):4878–97.
- [92] Amirjani A, Amlashi NB, Ahmadiani ZS. Plasmon-enhanced photocatalysis based on plasmonic nanoparticles for energy and environmental solutions: a review. ACS Appl Nano Mater. 2023;6(11):9085–123.
- [93] Wu B, Liu D, Mubeen S, Chuong TT, Moskovits M, Stucky GD. Anisotropic growth of TiO2 onto gold nanorods for plasmonenhanced hydrogen production from water reduction. J Am Chem Soc. 2016;138(4):1114–7.
- [94] Liu Y, Yu J, Lun Y, Wang Y, Wang Y, Song S. Ligand design in atomically precise copper nanoclusters and their application in electrocatalytic reactions. Adv Funct Mater. 2023;33(44):2304184.
- [95] Ghosh G. Graphene oxide-nanocomposite-based electrochemical sensors for the detection of organophosphate pesticides. Sensing of deadly toxic chemical warfare agents, nerve agent simulants, and their toxicological aspects. Amsterdam, Netherlands: Elsevier; 2023. p. 635–58.
- [96] Zhu S, Liang S, Gu Q, Xie L, Wang J, Ding Z, et al. Effect of Au supported TiO2 with dominant exposed {0 0 1} facets on the visiblelight photocatalytic activity. Appl Catal B: Environ. 2012;119:146–55.